

## Adsorbate induced core level shifts of transition metal surfaces

A Density Functional Theory study

**VIKTOR NILSSON**

Department of Applied Physics  
CHALMERS UNIVERSITY OF TECHNOLOGY  
Gothenburg, Sweden 2013



Thesis for the degree of Master of Science in Engineering Physics  
Examensarbete för civilingenjörsexamen i Teknisk fysik

# Adsorbate induced core level shifts of transition metal surfaces

A Density Functional Theory study

Viktor Nilsson



Division of Chemical Physics  
Department of Applied Physics  
Chalmers University of Technology  
Gothenburg, Sweden 2013

Adsorbate induced core level shifts of transition metal surfaces  
A Density Functional Theory study  
VIKTOR NILSSON

© VIKTOR NILSSON, 2013

Department of Applied Physics  
Chalmers University of Technology  
SE-412 96 Gothenburg, Sweden  
Telephone: +46 (0)31-772 10 00

Cover:

A silver slab (surface) with adsorbed oxygen, showing the unit cell used for the calculations. The XPS process is also illustrated. See sections 1.2 and 3.2.

Printed by: Chalmers Reproservice  
Göteborg, Sweden 2013

Adsorbate induced core level shifts of transition metal surfaces

Viktor Nilsson

Department of Applied Physics

Chalmers University of Technology, Gothenburg 2013

### Abstract

A shift in the core electron binding energy detected with X-ray photoelectron spectroscopy (XPS) gives insight into the local chemical configuration of atoms. Such information can be used, for instance, to determine the surface structure upon adsorption. By comparing the experimental spectra with theoretical predictions, the core level shifts can be attributed to specific atomic configurations.

In this thesis, core level shifts for metal surfaces upon adsorption have been computed by electronic structure calculations within density functional theory (DFT), using the software VASP.

The transition metals Ni, Cu, Ru, Rh, Pd, Ag, Cd, Pt and Au have been investigated in terms of their surface structure and adsorption sites for CO, H, O and S have been tested. Core level shifts for the hcp(0001)/fcc(111) and fcc(100) facets have been determined for each adsorbate. Since the involved mechanisms contributing to these energy shifts are difficult to decouple, trends among shifts as well as a model for explaining them have been sought.

A clear dependence on coordination number is seen, where the binding energy is lower for a lower coordination. Trends depending on element are also found. The shift upon adsorption is towards higher binding energies for almost all elements and adsorbates. Notable exceptions are Ag and Cd. The correlation between d-band centre shift and core level shift is confirmed whereas the common model of viewing charge transfer as a dominant effect for the shifts is found insufficient.

**Keywords:** DFT, density functional theory, XPS, ESCA, adsorption, core level binding energy



## Acknowledgements

First and foremost, thanks to my supervisor Henrik Grönbeck for a clear introduction to problems, for very helpful guidance always pointing me in the right direction, and for having time to discuss at the strangest hours.

Maxime for helping me to get started and being around both for questions on VASP and for discussions.

Simon for your attention to detail and willingness to discuss physics.

Anders for showing interest in my work and coming with suggestions for analysis.

The rest of the computational team: Adriana, Jakub, Oliver, Samira, and our group at Chemical Physics.

Jenny and Karin for feedback on the report.

The calculations were performed at the supercomputer centre C<sup>3</sup>SE at Chalmers, with CPU time provided through a SNIC grant.

Viktor Nilsson, Göteborg, 2013-06-27



# Contents

<b>Contents</b>	<b>i</b>
<b>List of Figures</b>	<b>iii</b>
<b>List of Tables</b>	<b>iv</b>
<b>1 Introduction</b>	<b>1</b>
1.1 Background . . . . .	1
1.2 Core level spectroscopy . . . . .	1
1.3 Core level shifts (CLS) . . . . .	3
1.3.1 Surface core level shifts (SCLS) . . . . .	3
1.3.2 Chemical shifts ( $\Delta$ SCLS) . . . . .	4
1.3.3 Theoretical models of core level shifts . . . . .	4
1.4 Purpose . . . . .	5
1.5 Objective . . . . .	5
1.6 Scope . . . . .	6
<b>2 Density Functional Theory (DFT)</b>	<b>7</b>
2.1 Computational environment . . . . .	9
<b>3 Properties derived from electronic structure</b>	<b>11</b>
3.1 Bulk calculations and convergence testing . . . . .	11
3.1.1 Lattice parameter . . . . .	12
3.1.2 Cohesive energy . . . . .	12
3.1.3 Bulk modulus . . . . .	13
3.2 Investigating surface structure . . . . .	14
3.2.1 Surface formation energy . . . . .	14
3.2.2 Adsorption energy and adsorption sites . . . . .	15
3.3 Surface core level shifts (SCLS) . . . . .	16
3.3.1 Model convergence (slab thickness and vacuum) . . . . .	17
3.3.2 Surface coverage . . . . .	17

3.3.3	Bader charge transfer analysis . . . . .	17
3.3.4	Density of states (DOS) and d-band shift . . . . .	18
<b>4</b>	<b>Results</b>	<b>19</b>
4.1	Bulk structure . . . . .	19
4.2	Surface structure . . . . .	22
4.2.1	Surface energy . . . . .	22
4.2.2	Adsorption sites . . . . .	23
4.3	Surface core level shifts and chemical shifts . . . . .	26
4.3.1	Convergence of SCLS . . . . .	26
4.3.2	SCLS . . . . .	28
4.3.3	Chemical shifts ( $\Delta$ SCLS) . . . . .	30
4.4	Bader charge transfer analysis . . . . .	32
4.5	Density of states (DOS) and d-band shift ( $\Delta\varepsilon_d$ ) . . . . .	34
4.5.1	Correlation $\Delta$ SCLS – $\Delta\varepsilon_d$ . . . . .	34
<b>5</b>	<b>Discussion</b>	<b>37</b>
5.1	Results . . . . .	37
5.2	Method . . . . .	38
5.3	Further studies . . . . .	38
<b>6</b>	<b>Conclusion</b>	<b>41</b>
	<b>Bibliography</b>	<b>45</b>
<b>A</b>	<b>Adsorption energies</b>	<b>47</b>

# List of Figures

1.1	Experimental XPS spectra . . . . .	2
1.2	Energy diagram showing the core levels and a SCLS . . . . .	3
1.3	Experimental XPS binding energies for palladium and silver . . . . .	6
1.4	Periodic table highlighting the investigated metals . . . . .	6
3.1	Convergence of cutoff energy and k-points . . . . .	12
3.2	Convergence of lattice parameter relaxation . . . . .	13
3.3	Calculation of Pd bulk modulus in ASE . . . . .	13
3.4	Illustration of model system with unit cell shown . . . . .	14
3.5	(2 × 2) surface cells showing adsorption sites . . . . .	15
3.6	SCLS calculation from total energies . . . . .	17
4.1	Crystal facets of In . . . . .	22
4.2	Adsorption energies for all sites and adsorbates . . . . .	24
4.3	Convergence of slab thickness . . . . .	26
4.4	Electron density difference for O on Pd . . . . .	27
4.5	Core level shifts of Pd for both kinds of surface atoms . . . . .	28
4.6	Core level shifts . . . . .	29
4.7	Trends in $\Delta$ SCLS . . . . .	30
4.8	Bader charge correlation – $\Delta$ SCLS vs $\Delta\rho$ . . . . .	32
4.9	DOS for O on 4d metals . . . . .	34
4.10	DOS for the Ni and Cu groups with adsorbed O . . . . .	35
4.11	Shift of d-band centre and chemical shift side by side . . . . .	35
4.12	$\Delta$ SCLS against $-\Delta\varepsilon_d$ for (111) surfaces . . . . .	36
4.13	$\Delta$ SCLS against $-\Delta\varepsilon_d$ for (100) surfaces . . . . .	36

# List of Tables

4.1	Lattice parameters . . . . .	20
4.2	Cohesive energies . . . . .	20
4.3	Bulk moduli . . . . .	21
4.4	Surface energies . . . . .	22
4.5	Surface energies for indium . . . . .	22
4.6	Adsorption energy in eV for H on Pd(100) . . . . .	23
4.7	Preferred adsorption sites . . . . .	23
4.8	Surface core level shifts (SCLS) . . . . .	28
4.9	Chemical shifts ( $\Delta$ SCLS) . . . . .	31
4.10	Charge transfer and d-band shift together with chemical shift . . . . .	33
A.1	CO on (100) . . . . .	47
A.2	H on (100) . . . . .	47
A.3	O on (100) . . . . .	48
A.4	S on (100) . . . . .	48
A.5	CO on (111) . . . . .	48
A.6	H on (111) . . . . .	49
A.7	O on (111) . . . . .	49
A.8	S on (111) . . . . .	50

# Chapter 1

## Introduction

In discussions of chemical bonding one generally distinguishes between core electrons and valence electrons. The chemical bond is made via the valence electrons through hybridisation and delocalisation. However, the core electrons are also affected by the changes in the valence orbitals.

Core level shifts are shifts in the binding energy of the core electrons that occur due to changes in the local environment of the atoms. The shifts can be used as chemical probes of effects such as adsorption of molecules on a surface. The theoretical prediction and study of these shifts using electron structure calculations is the subject of this thesis.

### 1.1 Background

The binding energy of core states can be measured with X-ray Photoelectron Spectroscopy (XPS). The method is site and element specific and is often used to characterise adsorbed molecules and atoms on surfaces with respect to chemical state and structure. The interpretation of experimental spectra is complicated by the complex photoemission process and generally needs support by theoretical calculations. Electron structure calculation using Density Functional Theory (DFT) is an established method for predicting structural and energetic properties of large quantum systems such as surfaces and atoms adsorbed at surfaces.

### 1.2 Core level spectroscopy

XPS as a tool for chemical analysis was pioneered by Kai Siegbahn in the mid 1960's<sup>[1]</sup> and is now routinely used in materials analysis.<sup>1</sup> It is used to characterise materials with respect to composition and structure. The fact that core states of atoms in different en-

---

<sup>1</sup>XPS is also called ESCA – Electron Spectroscopy for Chemical Analysis.

vironments appear with distinct peaks gives information that can not be obtained from, for example, mass spectrometry. Modern synchrotron X-ray sources give a resolution of core levels below 0.1 eV.

Figure 1.1a shows how different carbon atoms have a different binding energy depending on the local chemical surrounding. This is an example of the resolution achievable in XPS on molecules. The surface sensitivity of the method is illustrated in Figure 1.1b, where the spectra of clean and oxidised Pd(100) are shown. The oxidised surface has a surface-oxide, a PdO(101) monolayer that forms upon Pd(100) oxidation. Energies are much less separated than in the molecular example, so it is necessary to rely on deconvolution to extract information. Even so, theoretical calculations are usually needed to draw conclusions about the chemical details.

The red component in Figure 1.1b is the bulk signal, and the blue is from the surface. The negative offset of the surface with respect to bulk shows the negative surface core level shift of the Pd(100) surface. The green component in Figure 1.1c comes from Pd atoms coordinated with four oxygens in the overlayer, and the purple signal is from Pd bound to two oxygens. The blue surface signal comes from the first metallic layer and is shifted relative to the clean surface.

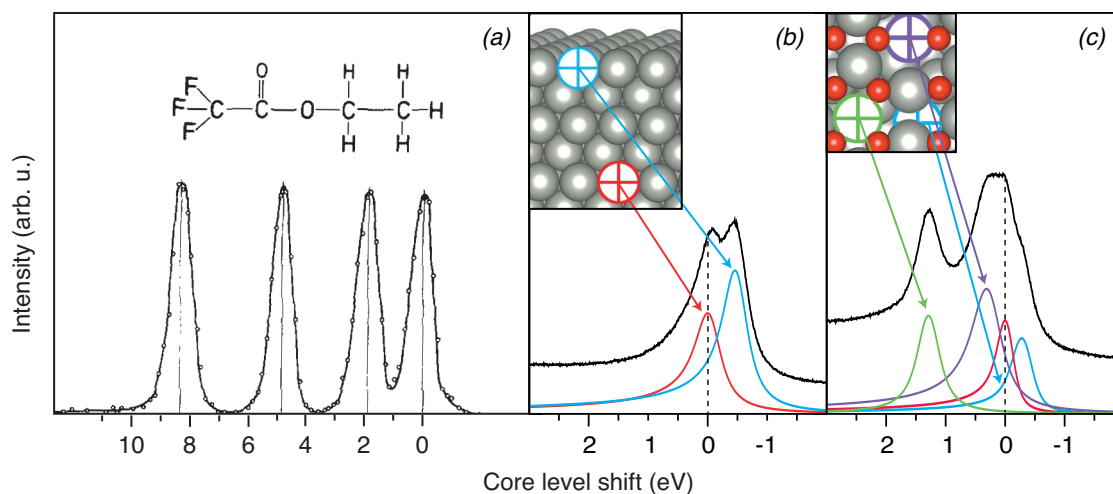


**Figure 1.1:** Experimental XPS spectra. Panel (a) shows the chemical splitting of carbon 1s binding energies in gas phase ethyl trifluoroacetate. Panel (b) shows the palladium 3d binding energy for the (100) surface. Panel (c) shows Pd(100) with a PdO(101) oxide overlayer. The coloured peaks are from Pd atoms with a chemical setting as highlighted (and explained above). Panel (a) is adapted from [2], (b) and (c) are from [3].

### 1.3 Core level shifts (CLS)

Binding energies of electrons in the inner atomic orbitals (core states) are measured by X-ray excitation. When a photon with energy  $\hbar\omega$  hits an atom it first does work against the binding energy  $E_B$ , which is defined as the work required to lift the electron to the Fermi level. To eject the electron to vacuum it also has to overcome the work function  $\Phi$  of the metal. What is left is the kinetic energy which is measured (Figure 1.2).

$$\hbar\omega = E_B + E_{\text{kin}} + \Phi$$

The binding energy is defined as positive; a larger binding energy corresponds to a more negative orbital energy  $\varepsilon$ . Energies are typically referenced to the Fermi level  $\varepsilon_F$ .

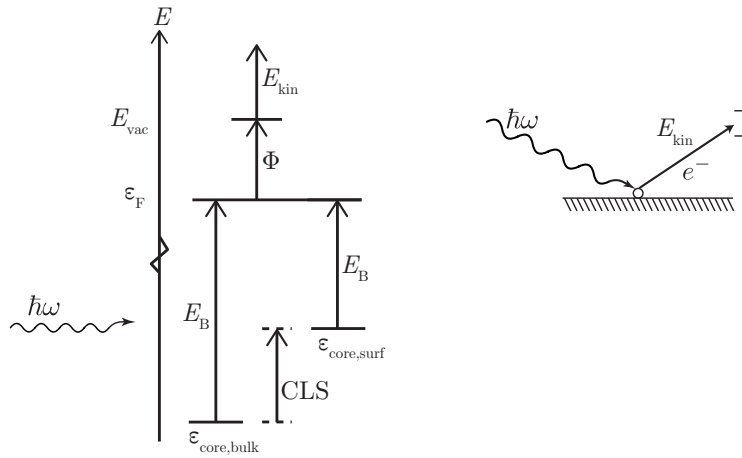


**Figure 1.2:** Energy diagram showing the core energy levels, Fermi energy, work function and a core level shift between surface and bulk atoms. On the right is an illustration of the process; a photon (with energy  $\hbar\omega$ ) ejects the electron ( $e^-$ ) from the surface.

We have seen that core energy levels of an atom are sensitive to its immediate surroundings, such as position in a structure. The core level shift (for a specific orbital, e.g. 3d in palladium) is defined as the core binding energy difference between two settings for the atom, and is positive for an increase in binding energy (Figure 1.2).

#### 1.3.1 Surface core level shifts (SCLS)

The surface core level shift or surface shift is the core level difference between bulk and surface atoms:

$$\text{SCLS} = E_{B,\text{surf}} - E_{B,\text{bulk}} \quad (1.1)$$

The bulk atom has a higher coordination number than the surface atom, but there are also surface reconstruction effects, both in the atomic positions and electronic structure.

The typical experimental SCLS for transition metals on the right side of the periodic table is towards lower binding energy at the surface, as illustrated in Figure 1.1b.

### 1.3.2 Chemical shifts ( $\Delta$ SCLS)

When atoms are adsorbed at the surface the charge landscape is modified, causing another shift of  $E_B$  as compared to the clean surface, as seen in Figure 1.1c. The chemical shift (eq. 1.2) is the difference between the surface shift of the clean surface and the surface shift with adsorbates. The bulk energy is unaffected by the adsorbates.

$$\Delta\text{SCLS} = \text{SCLS}(\text{bound}) - \text{SCLS}(\text{clean}) = E_{B,\text{surf}}(\text{bound}) - E_{B,\text{surf}}(\text{clean}) \quad (1.2)$$

### 1.3.3 Theoretical models of core level shifts

Shifts of the core levels with respect to a reference, usually the bulk atom for metals, are caused by different effects that partly counteract each other, making shifts difficult to analyse. This section reviews methods of explanation found in literature.

One approach is to consider the initial state, the charge distribution and electrostatics of the equilibrium system. This is the system on which the core-excitation takes place, and the core level binding energy is then usually obtained from the core state eigenvalues.

The final state picture views the system after core excitation (but before hole recombination) and includes screening of the core hole by the valence electrons, which causes a sometimes large correction to the binding energy not included in the ground state eigenvalue. The binding energy is obtained from the total energy difference between the electronically relaxed system with and without a core hole. This is closer to what is actually measured.

**Four electrostatic mechanisms** have been used in [4] to explain the shifts in terms of where charge is located relative to the core.

*Transfer of charge* from the substrate atom to the adsorbate, where missing (negative) charge in the valence orbital of the substrate atom causes the core electrons feel a positive potential ( $\sim 1/\langle r \rangle_{\text{val. orb.}}$ ) and gives rise to an increase in binding energy. This has traditionally been seen as the major contribution to the CLS[4].

*Electrostatic interaction* with adsorbates as a result of their extra charge causes the core electrons to feel a negative potential ( $\sim 1/d_{\text{bond}}$ ), lowering the binding energy. This counteracts the charge transfer effect. In addition, charges at the surface cause polarisation of the metal, which further influences  $E_B$ .

*Environmental charge density* accumulation from bond formation (wave function overlap) causes a shift in binding energy dependent on the coordination number (nearest neighbour count). Higher coordination gives more closely located charge and thus lower binding energy.

*Hybridisation* plays a similar role in moving charge by promoting electrons to orbitals with larger radii, resulting in an increased binding energy.

**The complete screening picture** has been discussed in [5]. The CLS can be expressed fully in terms of valence charge properties for a system with a core-ionised metal atom. If the binding energy of the core electron is referenced with respect to the Fermi level, the binding energy is seen as the difference between a pure piece of metal and one where the core electron is excited to the valence. We can thus consider an impurity atom with a core hole and an extra valence charge (can be approximated with an atom of atomic number  $Z+1$  in an environment of  $Z$ -atoms). The difference in total energy between this system and the pure metal gives the core binding energy.

The reason to use the complete screening picture is that the initial state or electrostatic treatment neglects all contributions arising in the excitation process[6]. The screening process is very fast, so the electrons have time to relax around the core hole before the emitted electron leaves the system. This is the framework that allows the calculations used in this thesis.

The fact that surface shifts are negative for late transition metals can be explained by the screening picture: Above half-filling, occupation of the d-band is in anti-bonding states. The core electron is removed and the extra electron, placed in the valence, is attracted by the charged core. In the screening configuration of the atom, it ends up in an anti-bonding orbital which does not like to participate in bonds to its neighbours. Since the surface atom has fewer neighbours, the repulsion of the core ionised atom is lower here.

## 1.4 Purpose

Since the mechanisms behind the core level shifts are difficult to unravel, full electron structure calculations are used to predict them. In particular, the shift of Ag upon oxygen adsorption is negative (i.e. gets lower binding energy) unlike its neighbouring metals (Figure 1.3). When sulphur is adsorbed on Ag, the shift is positive, which is what is expected for oxygen when treated with an electrostatic approach.

## 1.5 Objective

The main goal is to find a set of credible quantitative predictions of surface core level shifts for adsorbed molecules on relevant surfaces. In particular, metals close to Ag in the periodic table are of interest.

Unless the problem is irreducibly complicated, another aim is to find trends and construct a simple model describing the phenomenon. Using this model, the energy

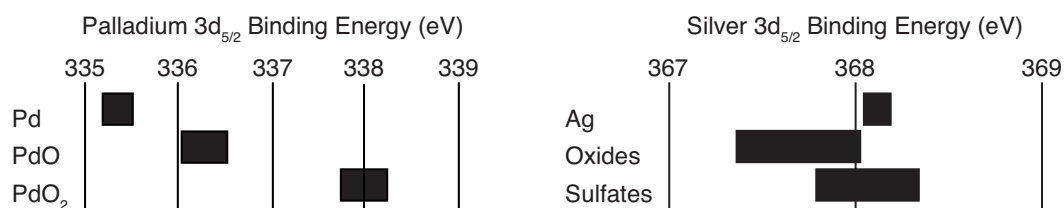


**Figure 1.3:** Experimental XPS binding energies for palladium and silver. Oxidised Pd has a higher binding energy than pure Pd. Oxidised Ag has lower binding energy whereas sulphur on silver (sulphates, also containing oxygen) can shift to higher binding energy. Adapted from Handbook of X-ray Photoelectron Spectroscopy[7].

shifts can be explained without having to resort to full electron structure calculations.

## 1.6 Scope

The study is purely theoretical, relying on well known computational methods. The project is restricted to the adsorbates oxygen, hydrogen, sulphur and carbon monoxide. The metals investigated are Ni, Cu, Pd, Ag, Pt and Au. When this gives reasonable results, the elements Ru, Rh, Cd and In in the 4d-period will be treated. Furthermore, only the most common crystal plane surfaces are considered, e.g. (111) and (100) for the fcc lattice.

hydrogen 1 <b>H</b>																	helium 2 <b>He</b>
lithium 3 <b>Li</b>	beryllium 4 <b>Be</b>											boron 5 <b>B</b>	carbon 6 <b>C</b>	nitrogen 7 <b>N</b>	oxygen 8 <b>O</b>	fluorine 9 <b>F</b>	neon 10 <b>Ne</b>
sodium 11 <b>Na</b>	magnesium 12 <b>Mg</b>											aluminium 13 <b>Al</b>	silicon 14 <b>Si</b>	phosphorus 15 <b>P</b>	sulfur 16 <b>S</b>	chlorine 17 <b>Cl</b>	argon 18 <b>Ar</b>
potassium 19 <b>K</b>	calcium 20 <b>Ca</b>	scandium 21 <b>Sc</b>	titanium 22 <b>Ti</b>	vanadium 23 <b>V</b>	chromium 24 <b>Cr</b>	manganese 25 <b>Mn</b>	iron 26 <b>Fe</b>	cobalt 27 <b>Co</b>	nickel 28 <b>Ni</b>	copper 29 <b>Cu</b>	zinc 30 <b>Zn</b>	gallium 31 <b>Ga</b>	germanium 32 <b>Ge</b>	arsenic 33 <b>As</b>	selenium 34 <b>Se</b>	bromine 35 <b>Br</b>	krypton 36 <b>Kr</b>
rubidium 37 <b>Rb</b>	strontium 38 <b>Sr</b>	yttrium 39 <b>Y</b>	zirconium 40 <b>Zr</b>	niobium 41 <b>Nb</b>	molybdenum 42 <b>Mo</b>	technetium 43 <b>Tc</b>	ruthenium 44 <b>Ru</b>	rhodium 45 <b>Rh</b>	palladium 46 <b>Pd</b>	silver 47 <b>Ag</b>	cadmium 48 <b>Cd</b>	indium 49 <b>In</b>	tin 50 <b>Sn</b>	antimony 51 <b>Sb</b>	tellurium 52 <b>Te</b>	iodine 53 <b>I</b>	xenon 54 <b>Xe</b>
caesium 55 <b>Cs</b>	barium 56 <b>Ba</b>	lutetium 71 <b>Lu</b>	hafnium 72 <b>Hf</b>	tantalum 73 <b>Ta</b>	tungsten 74 <b>W</b>	rhenium 75 <b>Re</b>	osmium 76 <b>Os</b>	iridium 77 <b>Ir</b>	platinum 78 <b>Pt</b>	gold 79 <b>Au</b>	mercury 80 <b>Hg</b>	thallium 81 <b>Tl</b>	lead 82 <b>Pb</b>	bismuth 83 <b>Bi</b>	polonium 84 <b>Po</b>	astatine 85 <b>At</b>	radon 86 <b>Rn</b>
francium 87 <b>Fr</b>	radium 88 <b>Ra</b>	lawrencium 103 <b>Lr</b>	rutherfordium 104 <b>Rf</b>	dubnium 105 <b>Db</b>	seaborgium 106 <b>Sg</b>	bohrium 107 <b>Bh</b>	hassium 108 <b>Hs</b>	meitnerium 109 <b>Mt</b>	ununnium 110 <b>Uun</b>	ununium 111 <b>Uuu</b>	ununium 112 <b>Uub</b>	unquadium 114 <b>Uuq</b>					

**Figure 1.4:** Periodic table highlighting the investigated metals.

## Chapter 2

# Density Functional Theory (DFT)

Solving the electron structure for real-world materials is a problem complicated by the facts that the electron–electron interaction is difficult to handle, and that quantum systems can only be solved exactly for one-electron systems. The full many-body Hamiltonian is

$$\hat{H} = -\frac{1}{2} \sum_i^N \nabla_i^2 - \sum_i^N V(\mathbf{r}_i) + \sum_{i < j}^N U(\mathbf{r}_i, \mathbf{r}_j)$$

where the first term describes kinetic energy, the second the external potential felt by each electron<sup>1</sup> and the last term contains interaction between electrons. The equation that should be solved is the Schrödinger equation

$$\hat{H}\psi = E\psi.$$

This problem is computationally expensive to solve up to the point that treating more than a few electrons becomes pointless even with supercomputers.

The interaction term contains Coulomb repulsion and other correlation effects. The Pauli exclusion principle stating that two electrons with the same spin<sup>2</sup> can not occupy the same state has to be accounted for, which is often implicitly done by expressing the wavefunction as a Slater determinant.

Methods exist to treat exchange and correlation approximately, DFT being a very popular alternative for solid state physics and surface chemistry, and Hartree–Fock-based methods being the other major variant. DFT solves the problem by replacing the many-body problem with a single-body problem for the electron density  $n(\mathbf{r})$ . Thanks to the Hohenberg–Kohn theorems[8] we can express the full wavefunction as a functional of the density

$$\Psi = \Psi[n(\mathbf{r})]$$

---

<sup>1</sup>under the Born–Oppenheimer approximation where atomic nuclei are regarded as fixed

<sup>2</sup>or rather two identical fermions

and the density  $n$  that minimises the energy functional  $E[n]$  of the system (with conserved electron count) gives the correct ground state.

To calculate the density the Kohn–Sham equations[9] are commonly used.

$$\tilde{H}\phi_i = \left( -\frac{1}{2}\nabla^2 - V_{\text{ext}}(\mathbf{r}) + \underbrace{\int d\mathbf{r}' \frac{n(\mathbf{r}')}{|\mathbf{r} - \mathbf{r}'|}}_{\text{Hartree}} + \underbrace{\int d\mathbf{r} \rho(\mathbf{r}) \epsilon_{\text{XC}}(n, \nabla n, \dots)}_{\text{XC}} \right) \phi_i = \varepsilon_i \phi_i \quad (2.1)$$

$$n = \sum_{i=1}^N |\phi_i|^2 \quad (2.2)$$

The Schrödinger equation for noninteracting electrons in an effective potential (2.1) is solved and  $n$  is given by summing over the single-electron (or Kohn–Sham) orbitals (2.2). The single-electron Hamiltonian  $\tilde{H}$  consists of single-electron kinetic energy, external potential (including nuclear charge), Hartree energy and XC energy. The Hartree term treats the classic electrostatic repulsion. The XC-term treats exchange interaction (accounting for the Pauli principle), Coulomb correlation effects, and additional kinetic energy.

The resulting density  $n$  is then equal to the true density of the interacting many-electron system, and the total energy is given by a functional of  $n$  where a large part is the sum of the Kohn–Sham (KS) eigenvalues  $\varepsilon_i$ . Note that the KS eigenvalues  $\varepsilon_i$  do not represent a physical quantity and the KS orbitals are not the wavefunctions of actual electrons.

The problem is now that the XC-functional is not exactly known and has to be approximated. One way is to assume that  $\epsilon_{\text{XC}}$  depends only on the local density at each point[10], which works for slowly varying densities. By also including the dependence on the local gradient we have the so called generalised gradient approximation (GGA) which is more accurate. The Perdew–Burke–Ernzerhof (PBE) functional [11] used for this work is of GGA type.

A basis set must be used for expansion of the wavefunctions into linear combinations. Examples are atomic orbitals (LCAO), Gaussians (GTO) or plane waves (which are used by the software in this thesis). When using plane waves, it is advantageous to use periodic boundary conditions. This causes the wavefunction to be periodic, which is well suited for bulk and surface calculations. Another benefit is that plane waves make a complete basis set – any state can be expressed in terms of it. A plane wave expansion (eq. 2.3), is truncated at an energy cutoff  $(\mathbf{k} + \mathbf{G}) < 2E_{\text{cut}}$  chosen high enough to approximate the ground state electronic structure to desired precision.

$$\psi_{\mathbf{k}}(\mathbf{r}) = \sum_{\mathbf{G}} c_{\mathbf{k},\mathbf{G}} e^{-i(\mathbf{k}+\mathbf{G})\cdot\mathbf{r}} \quad (2.3)$$

The concept of pseudopotentials is of great importance. By replacing the core electrons with an effective potential, we only have to solve the problem for the valence electrons. It also makes the potentials much smoother, reducing the number of plane wave terms needed to the point that the plane wave basis becomes usable. The potentials are constructed such that they ensure wavefunctions matching those of the full problem beyond a critical radius. One method of generating pseudopotentials is with the Projector Augmented-Wave method (PAW) [12].

Since the calculations are done in  $k$ -space, the number of  $k$ -points in the first Brillouin zone needed to represent the wavefunctions in the real space geometry must be determined. This is done by a convergence test. Performing calculations in  $k$ -space is beneficial for parallelisation since the plane waves are nonlocal in real space. Determination of properties such as total energy is done by a summation over  $k$ -points.

The occupation of orbitals in metals at 0 K drops sharply to zero at the Fermi level. This is a problem in the plane wave expansion since it would need a very high  $k$ -point density to be represented correctly. Smearing of the occupation is used to circumvent this, resulting in partial orbital occupancies corresponding to a small electronic temperature (there are still no phonons) which is reasonable for a metal. Even (unphysical) negative occupancies are used with some methods, but this is all just a trick to make the problem easier to solve.

For a more thorough introduction to DFT, see [13] or [14].

## 2.1 Computational environment

All calculations were performed with the Vienna Ab-initio Simulation Package (VASP) version 5.2.12[15] running on a cluster with 64-bit Intel CPUs. A plane wave basis expansion of  $\psi$  was used with PAW pseudopotentials[12] already known from ab initio calculations.

For indium, a pseudopotential that treats the 4d-band as valence in addition to 5s and 5p was chosen, since the relevance of including In in the study is the relation to the other 4d-metals. The number of electrons treated as valence for each species was H: 1; C: 4; O, S: 6; Ru: 8; Rh: 9; Ni, Pd, Pt: 10; Cu, Ag, Au: 11; Cd: 12; In: 13.

The core holes were created in the following core orbitals: for 3d-metals (Ni, Cu) in a 2p-state, for 4d-metals (Rh through Cd) in a 3d-state and for 5d-metals (Pd, Ag), the holes were created in a 4f-state.

The PBE[11] exchange-correlation functional was used. The Atomic Simulation Environment (ASE) was used to generate input files for VASP, to visually inspect the geometries and to calculate the bulk moduli. The analysis was done with a mix of homegrown scripts and Excel-spreadsheets.



## Chapter 3

# Properties derived from electronic structure

Before calculating core level shifts, the structure on which to perform them had to be chosen. Evaluation of surface and adsorption energies pointed towards setups more likely to occur in nature; the energetically most stable surfaces and adsorption sites will dominate in experiments.

Lattice parameter, cohesive energy and bulk modulus were compared with experimental values and with similar computational studies. As the next step, the surface structure was determined for a couple of cuts through the crystal structure. A slab of some atomic layers was constructed, and the surface energy was compared with experiments and theory.

Once the surface lattice was known, the adsorbates were placed in the positions with potential energy minima. By relaxing the adsorbed structure, they ended up in local minima. Different minima were investigated to find the globally stable configurations.

The surface core level shifts were computed as the difference in total energy between a core-excited atom in the bulk (in the middle of the slab) and in the surface. The shifts were determined both for pure surfaces and for the atoms close to adsorbed molecules.

### 3.1 Bulk calculations and convergence testing

The convergence of the cutoff energy was tested for Cu which is one of the more troublesome pseudopotentials to deal with (see Figure 3.1). A conservative value should be used, high enough for the most difficult of the considered systems. A cutoff of 420 eV was chosen, which should be enough for all the adsorbates and metals studied.

When new structures were introduced, a test of k-point convergence was done, and the grid was typically chosen such that the energy was converged to about 10 meV. The k-point spacing is dependent on cell size, so larger dimensions require fewer k-points.

Because of this, all surface calculations had only one k-point in  $z$ -direction (see fig 3.4 for a view of the surface system). Since hcp crystals work better if using an odd number of k-points, with one point centred in the  $\Gamma$  point, odd k-points were used throughout. An example of k-point convergence testing is shown in Figure 3.1.

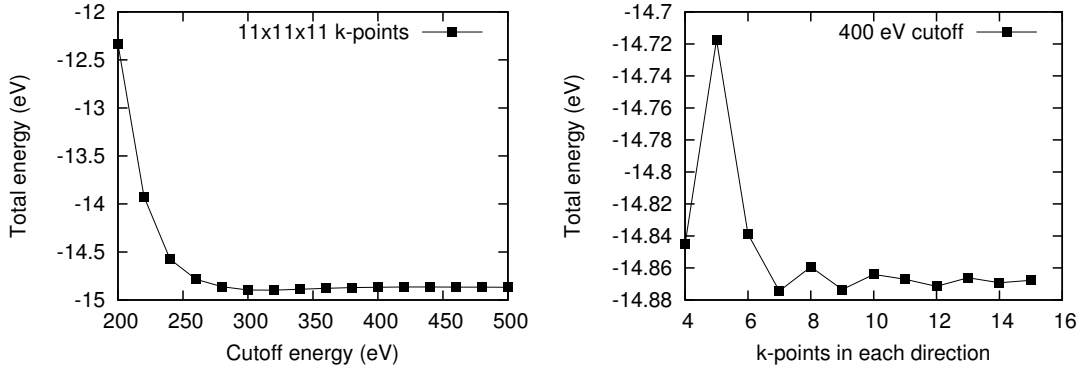


**Figure 3.1:** Convergence of cutoff energy (left) and k-points (right) for bulk Cu.

The smearing width of the occupation at the Fermi level (smearing of Fermi–Dirac distribution at 0 K) was lowered until the entropy in the system was below 1 meV/atom, according to the VASP manual. The required energetic convergence in the electronic self consistent loops was set to 5 significant digits.

### 3.1.1 Lattice parameter

The equilibrium lattice parameters were calculated by finding the stress tensor with a RMM-DIIS quasi-Newton method[16], and then iteratively updating the cell size until all forces were below 0.02 eV/Å. A change of cell shape was allowed for non-cubic cells, for the cubic cells a test was run to confirm that they could be constrained to one parameter. The convergence of energy is illustrated in Figure 3.2.

The calculated lattice parameter was not only used for comparison with experiments, but also as a starting point for generating all other structures.

### 3.1.2 Cohesive energy

The cohesive energy was calculated by subtracting the bulk energy per atom from the energy of an isolated atom.  $E_{\text{coh}} < 0$  if condensation is favourable.

$$E_{\text{coh}} = E_{\text{bulk}} - E_{\text{atom}}$$

The single atom was put in vacuum in a box of side 12 Å, and the energy was calculated with spin polarisation to match the experimental electron structure. Gaussian smearing

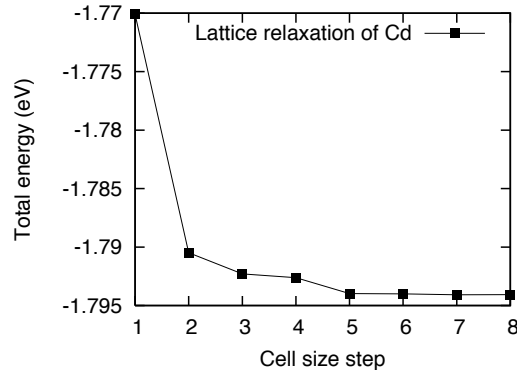


**Figure 3.2:** Convergence of lattice parameter relaxation.

was used[15]. Smearing corresponds to an electronic temperature which does not make sense in the isolated atom. The occupation of orbitals was therefore confirmed not to be fractional before treating the result as converged, otherwise smearing was decreased (increasing computational cost).

### 3.1.3 Bulk modulus

To determine the bulk modulus, a constitutive relation between cell volume and energy was fitted for a variation around an energy minimum, see Figure 3.3. The stabilised jellium equation of state[17] which is included in the ASE was used here.

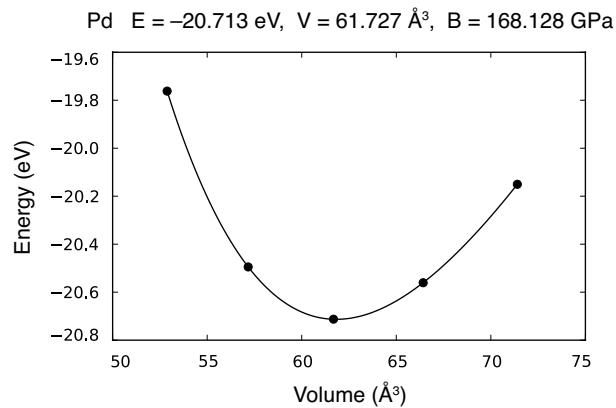


**Figure 3.3:** Calculation of Pd bulk modulus in ASE.

### 3.2 Investigating surface structure

The model used for surfaces is a slab with vacuum spacing to circumvent the periodic boundary condition in  $z$ -direction. The in-plane periodicity is utilised with as small surface cells as possible while still allowing for the desired surface structure (see Figure 3.4).

To make sure that calculated properties correspond to the equilibrium state (at 0 K), the structures were relaxed to an energy minimum within the used approximations. The relaxations were done by moving the atoms with the aforementioned quasi-Newton method or a Verlet algorithm that resets atom velocities when forces on them point in the opposite direction. The methods were applied until the convergence criterion of forces below  $0.01 \text{ eV}/\text{\AA}$  was reached.

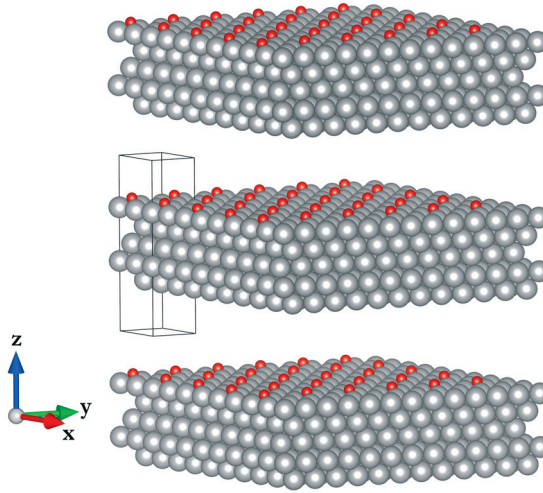


**Figure 3.4:** Illustration of a surface (slab) model system with unit cell shown. The cell is repeated periodically in all directions.

#### 3.2.1 Surface formation energy

Surface energies  $\sigma$  were computed to compare with experiments and to find the most stable surface cut. The surface energy calculations were performed using  $16 \text{ \AA}$  vacuum, 5 layers and  $(1 \times 1)$  surface cells with  $(13 \times 13 \times 1)$  k-points (except indium where  $(5 \times 5 \times 1)$  or  $(7 \times 7 \times 1)$  was enough because of a larger cell).

The surface energy was calculated as the difference between the slab total energy and the bulk energy

$$\sigma = \frac{1}{2A}(E_{\text{surf}} - NE_{\text{bulk}})$$

where  $N$  is the number of atoms in the slab unit cell,  $A$  is the surface area ( $= 1$  for atomic units) and the division by two is because the system contains two surfaces.

The surfaces investigated were the (111) and (100) for the materials with fcc structure. Ru and Cd have the hcp structure where the hcp(0001) surface was used. The hcp(0001) and fcc(111) are both close packed surfaces that look identical and will from now on be referred to as (111) for the sake of simplicity. Indium has a tetragonal crystal structure; the surface energy was calculated for its different facets but additional calculations were not performed since there is no structure equivalent of fcc(111), making energy comparisons with other elements difficult.

### 3.2.2 Adsorption energy and adsorption sites

The free energy  $F$  with which an adsorbate binds to a surface is obtained from the difference between the energy for the combined system and the sum of the two isolated systems:

$$F_{\text{ads}} = E(\text{slab with bound adsorbate}) - E(\text{clean slab}) - E(\text{free adsorbate}) \quad (3.1)$$

The  $E(\text{free adsorbate})$  can be calculated in two ways. Either it is the energy of a gas phase *atom* which is what is bound to the surface (except for CO) or it is the energy *per atom* of a gas phase *molecule*.

Binding to different positions of the surface was tested; the binding sites for (111) are shown in Figure 3.5. The (100) surface also has bridge and top positions, but only one hollow position.

All sites were tested for the adsorbates CO and H; for O and S the top position was excluded. The slab calculations were done with 14 Å vacuum and 5 layers in  $2 \times 2$  surface cells.

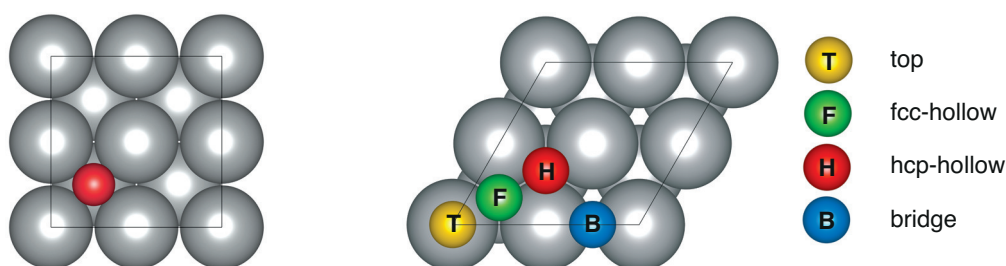


**Figure 3.5:** ( $2 \times 2$ ) surface cells for (100) on the left and (111) on the right. The possible adsorption sites for (111) are indicated. Note that the hollow sites coordinate to four surface atoms in the (100) surface and three in the (111).

### 3.3 Surface core level shifts (SCLS)

Core level shifts were determined for the adsorption structure that was energetically favourable for a majority of the systems – threefold fcc-hollow for (111) and fourfold hollow sites for (100).

The SCLS is calculated as a difference in total energies between two setups. For technical reasons it is not possible to calculate the binding energy of the core electrons. The total energy difference between a slab where a core electron is excited in a bulk atom (in the centre of the slab), and a slab where a core electron is excited in a surface atom matches the change in core binding energy (see Figure 3.6 and compare equation 3.2 with 1.1).

$$\text{SCLS} = E_{\text{tot}}(\text{surface core hole}) - E_{\text{tot}}(\text{bulk core hole}) \quad (3.2)$$

The slabs must be otherwise identical or the difference will contain errors.

VASP has a function for creating core holes (excitations). The valence electron density relaxes and screens the created core hole. This is the so called final state approximation or the complete screening picture. It includes final state effects on the binding energy, which are not seen by just looking at the ground state electronic structure without relaxation around core holes.

The core holes were created in the following core orbitals (which should most likely be excited by X-rays): for 3d-metals (Ni, Cu) in a 2p-state, for 4d-metals (Rh through Cd) in a 3d-state and for 5d-metals (Pd, Ag), the holes were created in a 4f-state.

The extra charge from when the core is ionised has to be dealt with if the system should continue to be charge neutral. The options available are to add a uniform background charge in the whole cell (as in the jellium model of core charges) or to add an electron at the Fermi level. For semiconductors or insulators an extra electron would appear in the conduction band, where it does not end up in reality, explaining the need for the background charge method. The method of an extra conduction electron matches the process described for the full screening picture and works very well for metals. It was used for all core level shift calculations.

There is also a possibility to excite fractional electrons (possible since we deal with densities) which is used to simulate the a transition state between the ground state and the excited state. This allows for a tuning of the calculated shifts compensating for the fact that emitted (measured) electrons may actually leave the system before the electronic relaxation is completed around the core hole. This possibility was not explored.

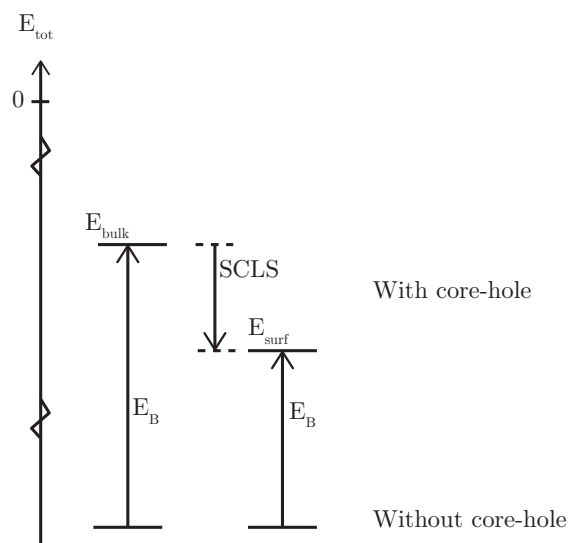


**Figure 3.6:** SCLS calculation from total energies.

### 3.3.1 Model convergence (slab thickness and vacuum)

To test convergence of the SCLS a Pd slab with 1/4 monolayer of adsorbed O and H respectively was set up with desired thickness (number of layers). The SCLS was determined for a surface atom bound to the adsorbate, and then for the clean atoms on the slab backside. Now, if the slab is metallic and has adsorbates only on the top surface, the back side should be unaffected because of screening. By comparing the SCLS of the back side atoms with the SCLS on a clean slab, the convergence of the model can be determined. From the same calculations, the convergence of each SCLS can also be seen.

The influence of vacuum spacing was also tested to make sure the wavefunctions do not overlap between the slabs. A thickness of 9 layers was required and that was used with 14 Å vacuum in all SCLS calculations.

### 3.3.2 Surface coverage

The surface cell used for SCLS was  $(2 \times 2)$  with an adsorbate surface coverage of 0.25 monolayers (in hollow positions). One core hole was created in the slab (and with periodic boundary conditions this also translates to a 0.25 coverage of core holes – which is probably high in comparison with experiments).

### 3.3.3 Bader charge transfer analysis

Bader analysis[18] assigns charge to the closest atoms by inserting dividing surfaces at the density minima between them, somewhat like the construction of a Wigner-Seitz cell

but with distances determined by the charge. Bader analysis was performed using the grid-based method without lattice bias[19], and the total number of assigned electrons was verified to differ by less than 0.0001 from the known number in the system. The charge on adsorbates and bound atoms was compared with the charge of neutral atoms to show how charge was transferred in the bonds.

### 3.3.4 Density of states (DOS) and d-band shift

The density of states of specific atoms was retrieved directly from VASP. The centroid energy for the d-band (DOS for the valence d-electrons) of the bound surface atoms was compared with that of a clean backside atom. This gives a d-band shift, explicitly given by

$$\Delta\varepsilon_d = \varepsilon_{d(\text{bound})} - \varepsilon_{d(\text{clean})} = \frac{\int e \cdot \text{DOS}_{\text{bound}}(e) de}{\int \text{DOS}_{\text{bound}}(e) de} - \frac{\int e \cdot \text{DOS}_{\text{clean}}(e) de}{\int \text{DOS}_{\text{clean}}(e) de}$$

where the integration is done over all states, including those above the Fermi level.

# Chapter 4

## Results

### 4.1 Bulk structure

Bulk calculations are found to follow experimental data rather closely across the elements. Constant offsets are expected since the models and functionals used are not perfect representations of the physical systems.

**Lattice parameter** The lattice parameters obtained from bulk calculations are given in Table 4.1. Relative errors compared with experiments are below 2.5 % for all elements.

**Cohesive energy** Cohesive energies are shown in Table 4.2. Ni did not converge in gas phase (single atom).

**Bulk modulus** Bulk moduli are shown in Table 4.3.

**Table 4.1:** Bulk lattice parameter  $a_0$  in Å. The relative errors are compared with experimental values  $(a_{\text{DFT}} - a_{\text{exp}})/a_{\text{exp}}$ . Experimental and theoretical reference from [20] except experimental data for Ru, Cd and In from [21] and theoretical data for In (using the similar PW91 functional instead of PBE) from [22].

	Calculated	Expt. ref.	Theor. ref.	Rel. error
Ni	3.52	3.524	3.52	-0.1%
Cu	3.63	3.615	3.63	0.5%
Ru a	2.73	2.71		0.6%
Ru c	4.30	4.28		0.6%
Rh	3.84	3.798	3.83	1.2%
Pd	3.95	3.881	3.95	1.8%
Ag	4.16	4.069	4.15	2.2%
Cd a	3.03	2.98		1.5%
Cd c	5.71	5.62		1.5%
In a	3.31	3.25	3.30	1.7%
In c	5.03	4.95	5.09	1.6%
Pt	3.98	3.923	4.00	1.4%
Au	4.17	4.079	4.18	2.3%

**Table 4.2:** Cohesive energies in eV/atom. All experimental values from [21] and theoretical reference [23] except Cu, Rh, Pd and Ag from [24].

	Calculated	Expt. ref.	Theor. ref.	Rel. error
Ni		4.44	4.87	
Cu	3.48	3.49	3.48	-0.4%
Ru	6.67	6.74	6.67	-1.0%
Rh	5.63	5.75	5.72	-2.1%
Pd	3.70	3.89	3.71	-4.9%
Ag	2.49	2.95	2.52	-15.6%
Cd	0.73	1.16	0.73	-36.7%
In	2.32	2.52		-8.1%
Pt	5.45	5.84	5.50	-6.7%
Au	2.99	3.81	2.99	-21.6%

**Table 4.3:** Bulk moduli in GPa. Experimental and theoretical reference from [20] except experimental data for Ru, Cd, In from [21] and theoretical data for Ru and Cd from [23].

	Calculated	Expt ref.	Theor. ref.	Rel. error
Ni	196	184	200	6.4%
Cu	138	133	141	3.4%
Ru	312	321	308	-2.7%
Rh	255	269	259	-5.2%
Pd	168	195	170	-13.8%
Ag	90	109	91	-17.1%
Cd	43	47	50	-8.6%
In	37	41		-11.1%
Pt	249	277	234	-10.1%
Au	139	167	131	-17.1%

## 4.2 Surface structure

### 4.2.1 Surface energy

The calculated surface energies  $\sigma$  are shown in Table 4.4 except indium which is in Table 4.5. The PBE functional is known to underestimate the surface energies [20], but the resulting trend follows the experimental data well. The (111) surface which is more closely packed has a lower energy than the (100) surface, as expected. Species with close to filled or filled shells have lower surface energy.

**Table 4.4:** Surface energies in  $\text{J}/\text{m}^2$ . (111) experimental and theoretical reference [20] with original experimental data from [25].

	$\sigma(111)$	Expt. ref.	Theor. ref.	$\sigma(100)$
Ni	1.89	2.38	1.98	2.20
Cu	1.28	1.79	1.36	1.44
Ru	2.61			
Rh	2.02	2.66	0.80	2.33
Pd	1.32	2.00	1.40	1.49
Ag	0.72	1.25	0.78	0.80
Cd	0.18			
Pt	1.54	2.49	1.52	1.84
Au	0.70	1.51	0.59	0.86

**Table 4.5:** Surface energies for indium.

Facet	In(101)	In(100)	In(001)	In(110)
$\sigma$ ( $\text{J}/\text{m}^2$ )	0.26	0.36	0.31	0.41

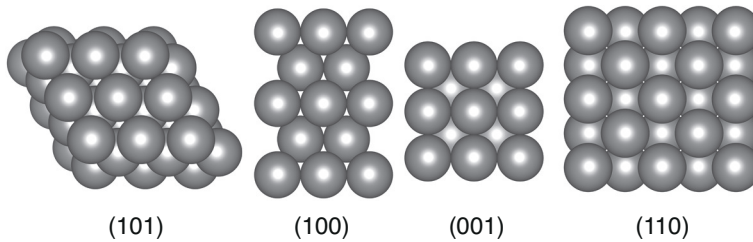


**Figure 4.1:** Crystal facets of In.

### 4.2.2 Adsorption sites

Adsorption energies were calculated with a 5-layer slab. The results are shown in Figure 4.2 and in appendix A.

All adsorbates bind with a negative energy with respect to free atoms (not applicable for CO). This means that the adsorbates bind to the surface in a local energy minimum. Some adsorbates do not dissociate on the surface, but the prepared structure is still stable (the binding in molecular phase is stronger than to the surface). This is the case for H/Ag and H/Au on both facets, H/Cd(0001) and O/Au(100). CO does not bind at all on Cd(0001).

Binding in hollow positions is stronger on the (100) surface. Binding in top and bridge positions is similar between the surfaces.

The strongest adsorption site is recorded for each adsorbate–metal combination, e.g. hollow is preferred for H on Pd(100) as in Table 4.6. The frequency of a site being preferred is shown in Table 4.7. Note that the “best” site is sometimes insignificantly better than another, e.g. fcc and hcp may differ with less than 1 meV. This is however not a problem, since this was done just to decide on which site the SCLS were to be calculated.

**Table 4.6:** Adsorption energy in eV for H on Pd(100)

	Site	$F_{\text{molec}}$	$F_{\text{atom}}$
	<i>hollow</i>	-0.462	-2.727
Pd	bridge	-0.433	-2.698
	top	0.022	-2.243

**Table 4.7:** Preferred adsorption sites.

(111)				(100)		
top	fcc-hollow	hcp-hollow	bridge	top	hollow	bridge
2	22	9	2	1	18	9

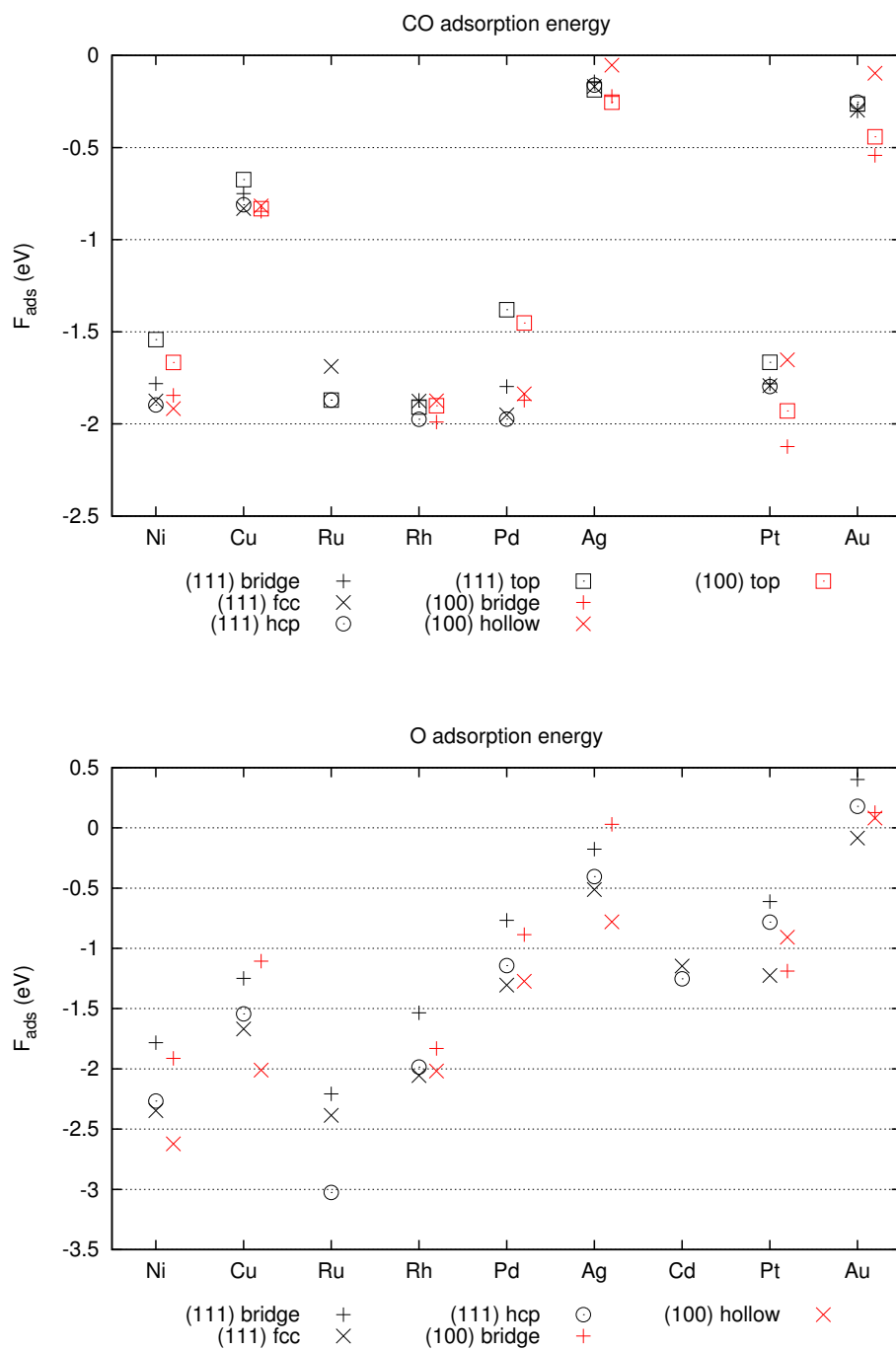
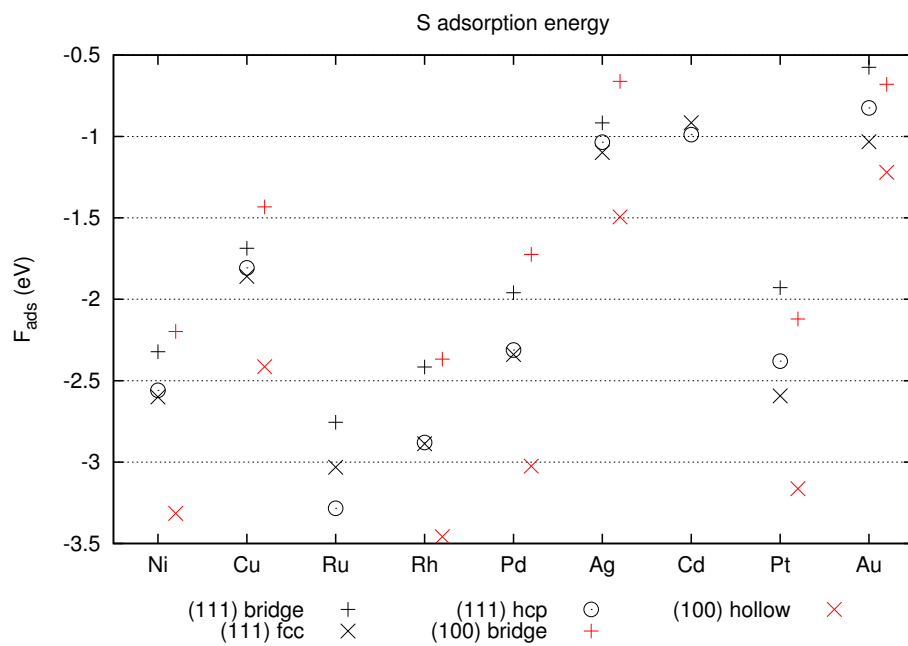
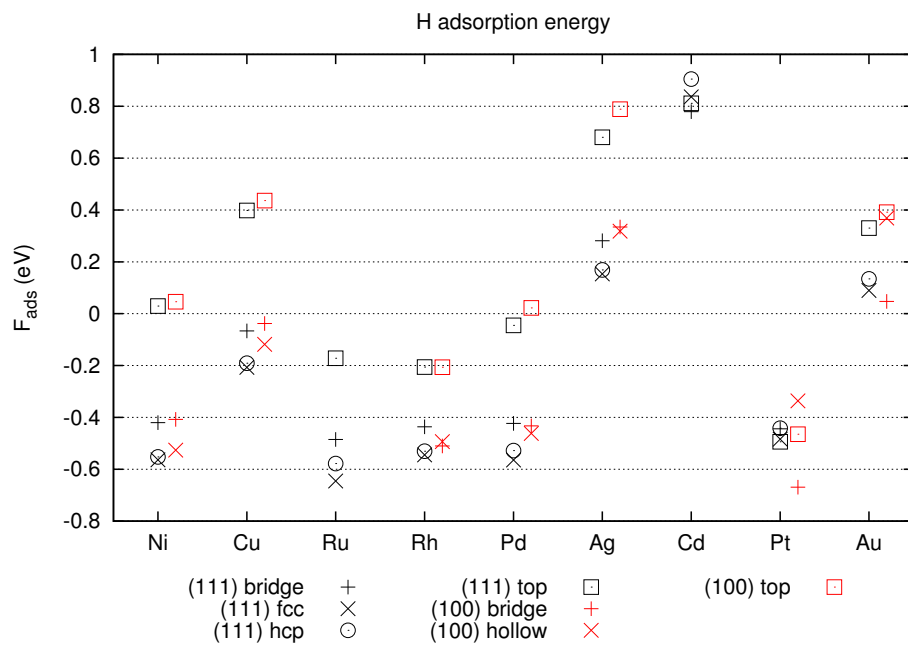


**Figure 4.2:** Adsorption energies relative to molecular gas phase (as opposed to free atomic adsorbates). Missing points indicate either that the adsorbate does not bind or that it falls down in the neighbouring hollow site.



### 4.3 Surface core level shifts and chemical shifts

#### 4.3.1 Convergence of SCLS

Convergence testing of SCLS with H and O on Pd showed that a 5-layer slab is not enough to fully converge the results. With 9 layers the SCLS is converged to within 0.01 eV. The difference in SCLS between the clean backsides of adsorbate-covered slabs and completely clean slabs is also converged to within 0.01 eV with 9 layers. (Figure 4.3). This difference is below 0.03 eV for all SCLS calculations except O on Cd(0001), which has a difference of 0.07 eV and CO on Pt(100), which differs with 0.04 eV.

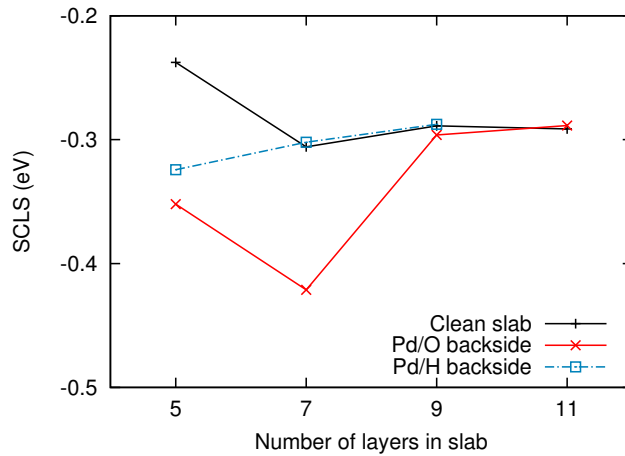


**Figure 4.3:** Convergence of slab thickness. Top unbound are the atoms not neighbouring the adsorbate on the surface with adsorbates in fcc-hollow.

Charge analysis (Figure 4.4) shows the reason why 5 layers were not enough; the bulk reference atom is affected by the adsorbate. By subtracting the charge of a clean Pd slab and atomic oxygen from the charge of the bound structure, only polarisation effects due to bond formation will show.

$$\Delta n = n(\text{Pd with bound O}) - n(\text{clean Pd}) - n(\text{O})$$

An isosurface at  $\Delta n = 0.002$  (Figure 4.4) shows a polarisation of the middle layer, where our bulk reference core hole is created.

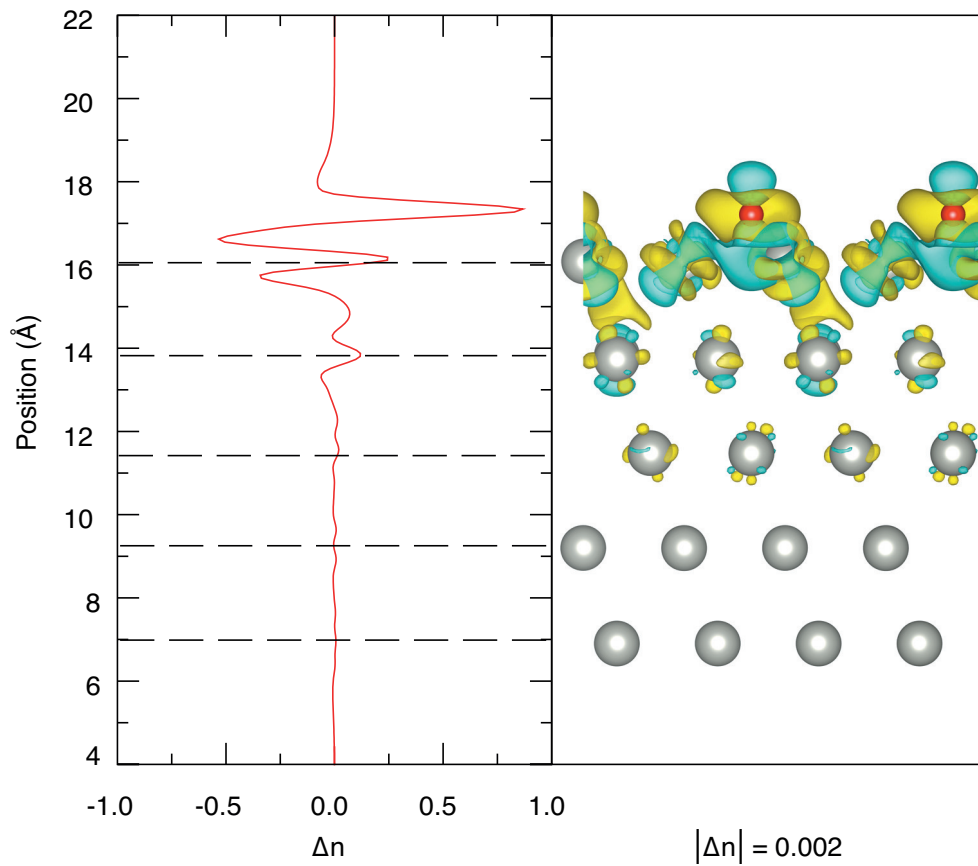


**Figure 4.4:** Electron density differences  $\Delta n$  for O on Pd. On the left: integrated over in-plane coordinates  $x$  and  $y$  to show  $\Delta n$  as a function of depth. The positions of slab layers are indicated with dashed lines. Coordinates are relative to cell boundary including vacuum spacing. On the right: charge density difference isosurface at  $|\Delta n| = 0.002$ . Yellow is positive (increase in electron density) and blue is negative.

## 4.3.2 SCLS

All surface shifts are shown in Table 4.8 and Figure 4.6. For the (111) facet, only the shifts of atoms bound to adsorbates are shown. For (100) there is only one kind of surface atom, always neighbouring the adsorbate. In Figure 4.5, the shifts of unbound surface atoms are shown as an example.

Almost all of the shifts are negative, that is towards lower core binding energy at the surface. Generally, the shifts are less negative for the (111) surface and they increase along the periods. A notable deviation arises with the large positive SCLS in the Ni-group (Ni, Pd, Pt) with adsorbed O or S; another exception is the strong negative shift of Rh. The difference between the two facets is smaller for the Cu-group. For Ag and Cd, the SCLS is very small in absolute numbers.

**Table 4.8:** Surface core level shifts (SCLS) in eV for 9 layer slabs with adsorbate coverage of 1/4 monolayer in fcc-hollow (111) and hollow positions (100).

	(111)					(100)				
	CO	H	O	S	Clean	CO	H	O	S	Clean
Ni	0.112	-0.139	0.182	0.212	-0.253	-0.187	-0.384	-0.302	-0.111	-0.474
Cu	0.219	-0.048	-0.243	0.029	-0.245	0.058	-0.109	-0.408	-0.115	-0.298
Ru	-0.322	-0.308	-0.115	-0.188	-0.369					
Rh	-0.349	-0.401	-0.083	-0.102	-0.481	-0.590	-0.669	-0.477	-0.445	-0.702
Pd	0.362	-0.031	0.443	0.609	-0.288	-0.001	-0.233	-0.087	0.252	-0.345
Ag	0.087	0.020	-0.351	-0.074	-0.127	0.036	0.015	-0.361	-0.106	-0.093
Cd		-0.011	-0.227	-0.109	-0.058					
Pt	0.064	-0.191	0.256	0.398	-0.364	-0.179	-0.392	-0.236	-0.003	-0.469
Au	0.180	-0.059	-0.298	0.012	-0.364	-0.073	-0.163	-0.465	-0.110	-0.378

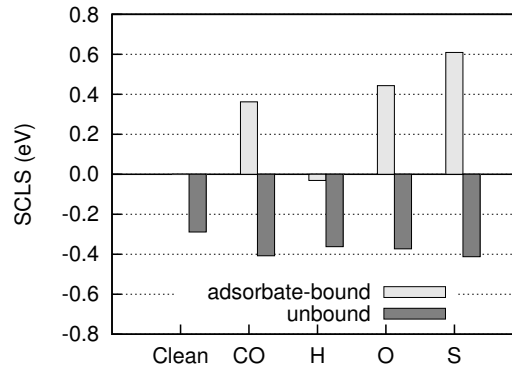


**Figure 4.5:** Core level shifts of Pd(111) for both kinds of surface atoms.

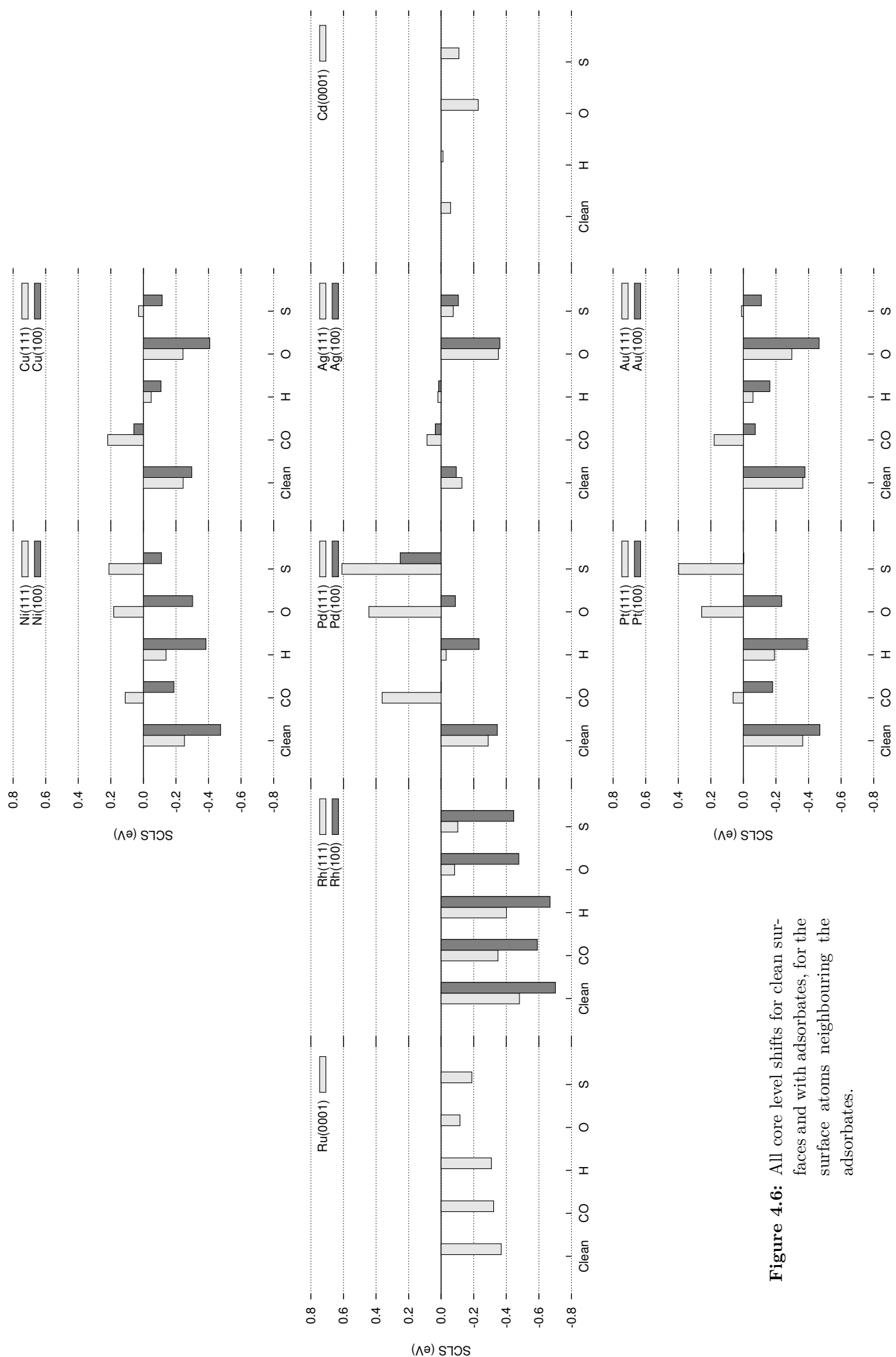


**Figure 4.6:** All core level shifts for clean surfaces and with adsorbates, for the surface atoms neighbouring the adsorbates.

### 4.3.3 Chemical shifts ( $\Delta$ SCLS)

The surface shift with adsorbate minus the clean surface shift is denoted  $\Delta$ SCLS and is shown in Table 4.9. Again the shifts are more positive for the (111) surfaces. S gives stronger shifts than O, and the shifts caused by H are very small.

With O and S on 3d-metals (Ni, Cu) and 5d-metals (Pt, Au), moving right in the period gives a larger shift, whereas with H and O the shift decreases. The 4d-metals behave differently; moving from Rh to Pd gives an increased shift and continuing from Pd to Ag gives a decreased shift, for all four adsorbates. See Figure 4.7

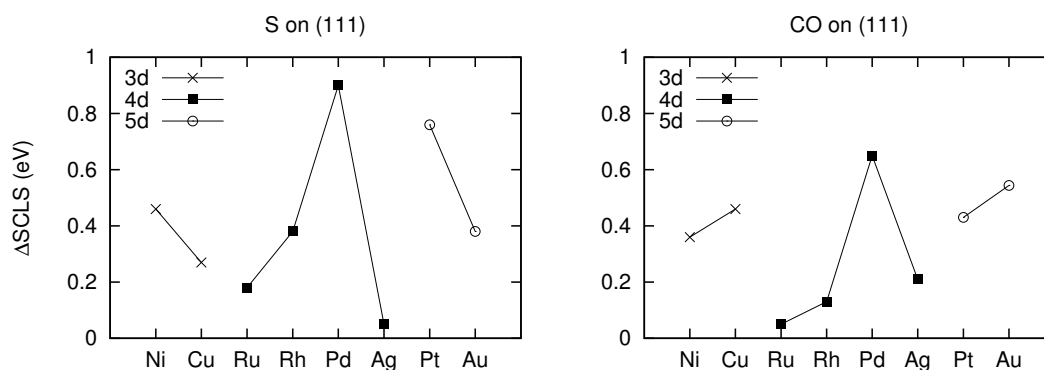


**Figure 4.7:** Trends in  $\Delta$ SCLS. Note how the shifts for 3d and 5d-metals decrease as you move right with adsorbed S whereas it increases with adsorbed CO. Also note that the 4d-metals show a similar trend in the two figures.

The negative shift for O on Ag(111) is reproduced, and is also seen with O or S on Cd. For the (100) facet, O/Cu and O/Au as well as S/Ag also show negative shifts.

Moving down the group of Ni, the very large shift for Pd causes a pattern of low–high–low. In the Cu group, the tiny shift of Ag gives the opposite pattern of high–low–high.

**Table 4.9:** Chemical shifts ( $\Delta$ SCLS) in eV for 9 layer slabs with adsorbate coverage of 1/4 monolayer in fcc-hollow (111) and hollow positions (100).

	(111)				(100)			
	CO	H	O	S	CO	H	O	S
Ni	0.364	0.114	0.435	0.464	0.287	0.090	0.172	0.363
Cu	0.463	0.197	0.001	0.274	0.356	0.189	-0.110	0.182
Ru	0.047	0.060	0.254	0.181				
Rh	0.132	0.080	0.398	0.379	0.112	0.033	0.225	0.257
Pd	0.651	0.257	0.732	0.898	0.344	0.112	0.257	0.596
Ag	0.215	0.147	-0.224	0.053	0.129	0.108	-0.268	-0.013
Cd		0.047	-0.169	-0.051				
Pt	0.427	0.173	0.620	0.762	0.290	0.077	0.234	0.467
Au	0.544	0.305	0.067	0.377	0.305	0.215	-0.087	0.267

#### 4.4 Bader charge transfer analysis

The charge change  $\Delta\rho$  is the average charge change with respect to bulk on the adsorbate-bound surface atoms (in units of elementary charges, positive number corresponds to loss of electrons).  $\Delta\rho$  is plotted against  $\Delta\text{SCLS}$  in Figure 4.8. No strong correlations are seen except for in sulphur, which shows less increase in binding energy when more electrons disappear. This is the opposite behaviour from what would be expected if charge transfer were a dominating cause for the chemical shift. The results for each metal are shown in Table 4.10.

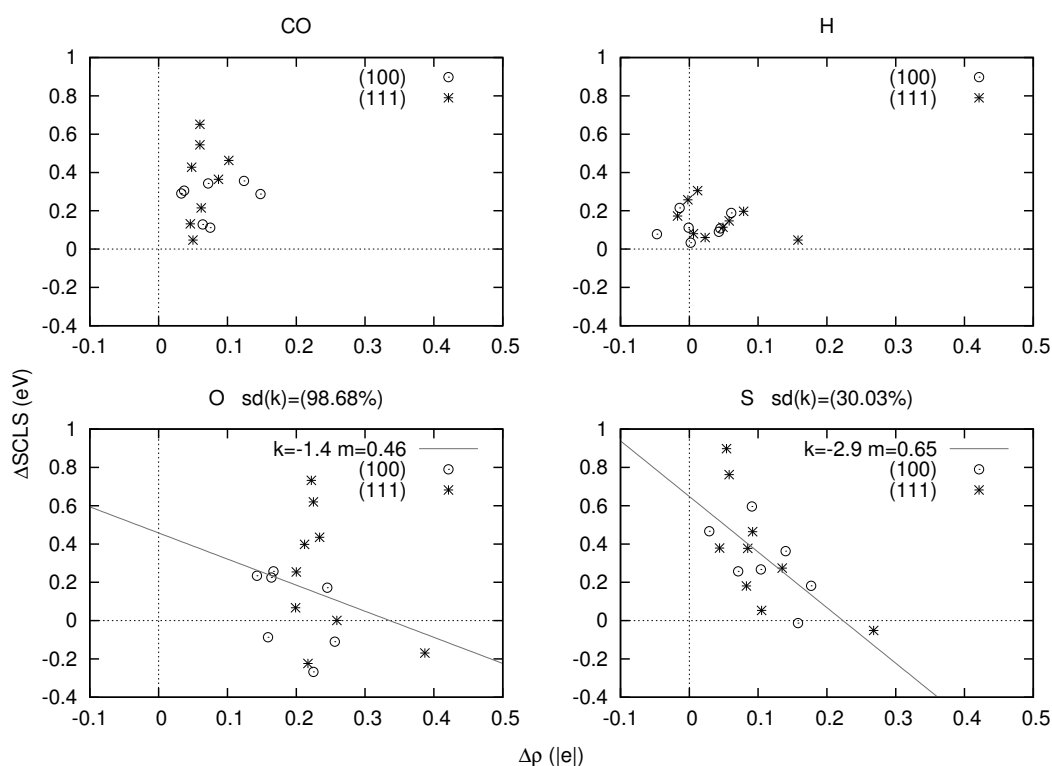


**Figure 4.8:** The chemical shift  $\Delta\text{SCLS}$  is plotted against  $\Delta\rho$ , which is the charge change on the atom on which the CLS is calculated.

**Table 4.10:** Chemical shift  $\Delta\text{SCLS}$  (eV), d-band shift  $\Delta\varepsilon_d$  (eV) and charge change  $\Delta\rho$  ( $|e|$ ).

Adsorbate	$\Delta\text{SCLS}$	(111)			(100)		
		$\Delta\varepsilon_d$	$\Delta\rho$	$\Delta\text{SCLS}$	$\Delta\varepsilon_d$	$\Delta\rho$	
Ni	CO	0.364	-0.006	0.087	0.287	-0.003	0.148
	H	0.114	0.005	0.049	0.090	0.021	0.043
	O	0.435	-0.248	0.234	0.172	-0.117	0.245
	S	0.464	-0.208	0.092	0.363	-0.078	0.140
Cu	CO	0.463	-0.429	0.102	0.356	-0.329	0.124
	H	0.197	-0.185	0.079	0.189	-0.104	0.061
	O	0.001	-0.212	0.259	-0.110	-0.030	0.256
	S	0.274	-0.317	0.135	0.182	-0.182	0.177
Ru	CO	0.047	-0.209	0.050			
	H	0.060	-0.083	0.023			
	O	0.254	-0.286	0.200			
	S	0.181	-0.330	0.083			
Rh	CO	0.132	-0.249	0.046	0.112	-0.171	0.075
	H	0.080	-0.133	0.006	0.033	-0.067	0.002
	O	0.398	-0.285	0.212	0.225	-0.112	0.164
	S	0.379	-0.334	0.044	0.257	-0.245	0.071
Pd	CO	0.651	-0.319	0.060	0.343	-0.152	0.072
	H	0.257	-0.143	-0.002	0.112	-0.041	-0.001
	O	0.732	-0.482	0.222	0.257	-0.213	0.167
	S	0.898	-0.657	0.054	0.596	-0.428	0.091
Ag	CO	0.215	-0.229	0.062	0.129	-0.166	0.064
	H	0.147	-0.144	0.058	0.108	-0.086	0.045
	O	-0.224	0.182	0.217	-0.268	0.180	0.225
	S	0.053	-0.072	0.105	-0.013	-0.033	0.158
Cd <sup>a</sup>	H	0.047	-0.101	0.158			
	O	-0.169	0.348	0.387			
	S	-0.051	0.129	0.268			
Pt	CO	0.427	-0.285	0.048	0.290	-0.087	0.033
	H	0.173	-0.168	-0.017	0.078	-0.012	-0.047
	O	0.620	-0.512	0.225	0.234	-0.195	0.143
	S	0.762	-0.685	0.058	0.467	-0.354	0.029
Au	CO	0.544	-0.496	0.060	0.305	-0.248	0.037
	H	0.305	-0.286	0.012	0.215	-0.165	-0.014
	O	0.067	-0.263	0.199	-0.087	0.002	0.159
	S	0.377	-0.440	0.085	0.267	-0.281	0.104

<sup>a</sup>: CO on Cd did not converge in the relaxation process.

## 4.5 Density of states (DOS) and d-band shift ( $\Delta\varepsilon_d$ )

The projected density of states on valence orbitals of adsorbate-bound surface atoms and clean backside atoms were visually inspected and some findings are illustrated in Figure 4.9. States from adsorbates show up on the bound surface atoms, they often appear in pairs. Often only one of the two peaks is below  $\varepsilon_F$  ( $E = 0$ ) but sometimes (as shown for Ag) they are both below  $\varepsilon_F$ . Moving right along the period (down in Figure 4.9), the d-bands lie deeper.

In Figure 4.10, moving down the groups, Ag has a considerably deeper d-band than Cu and Au. Again Cu is deeper than Ni and Au is deeper than Pt, which also means that more of their d-bands are occupied.

Broadening of d-bands on adsorption is seen clearly for Pd in Figure 4.9. The broadening is generally stronger for the elements to the left in the period, and stronger with O and CO than with H or S.

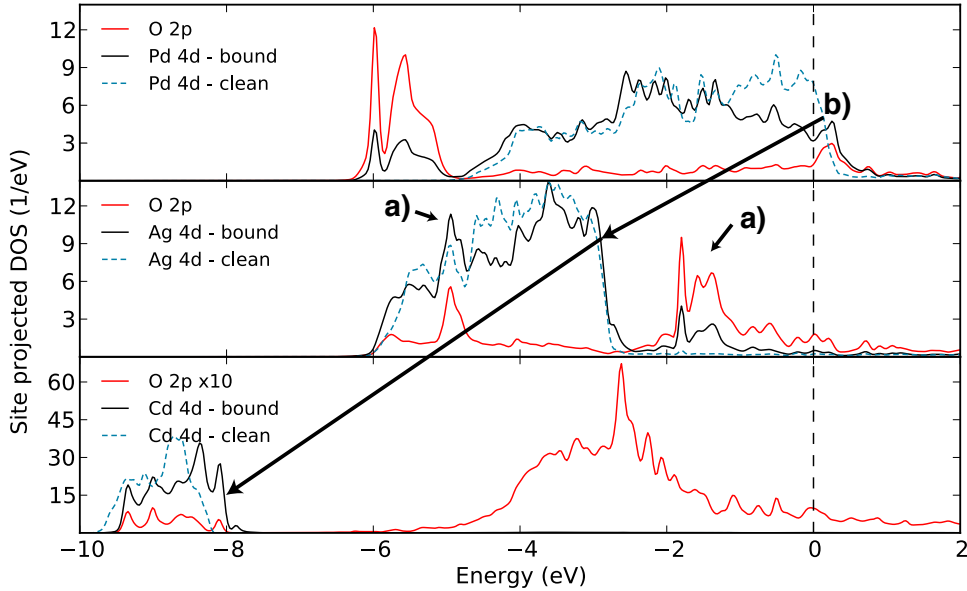


**Figure 4.9:** DOS for O on 4d metals. <sup>a)</sup>A pair of new states, here both below  $\varepsilon_F$ . <sup>b)</sup>d-bands are deeper for the heavier elements.

### 4.5.1 Correlation $\Delta\text{SCLS} - \Delta\varepsilon_d$

By inspecting the signs of the chemical shifts and contrasting them with features in the DOS, new states below the original d-band are found to coincide with a positive  $\Delta\text{SCLS}$ . The measure  $\Delta\varepsilon_d$  introduced in section 3.3.4 is calculated for all elements and shown in Table 4.10. When plotted along the periods, trends similar to those in  $\Delta\text{SCLS}$  are seen,

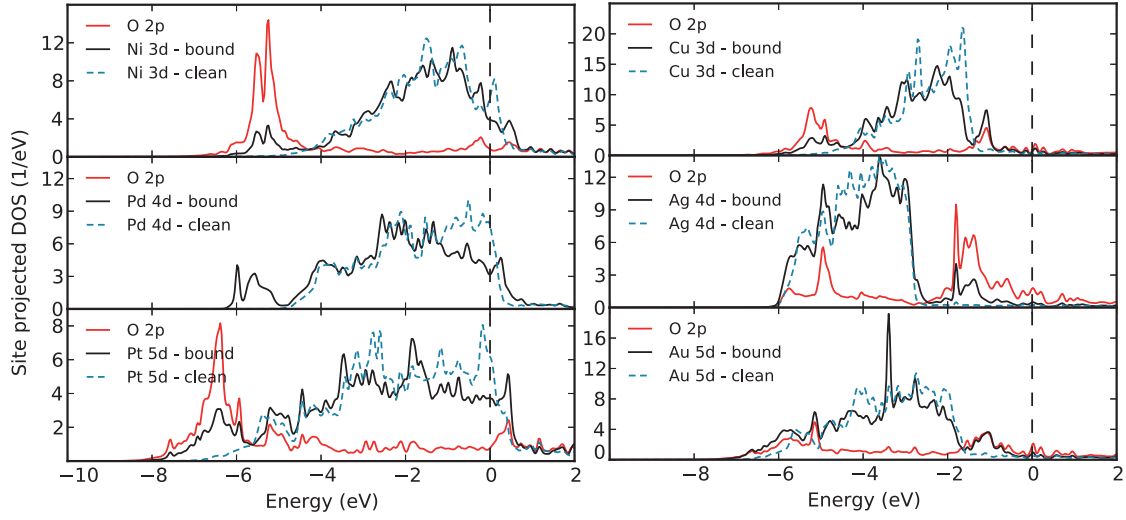


**Figure 4.10:** DOS for the Ni and Cu groups with adsorbed O. Note that the d-bands intersect  $\varepsilon_F$  for the left group while the right group’s d-band lies deeper. Also note that Ag initially (dashed) lies much deeper than Cu and Ag.

as shown in Figure 4.11. Despite the inability to match the negative  $\Delta\text{SCLS}$  of Cu and Au in this particular case, the qualitative similarities are striking.  $-\Delta\varepsilon_d$  plotted against  $\Delta\text{SCLS}$  in Figures 4.12 and 4.13 shows a good, almost 1:1 correspondence across the elements. The linear fits cut almost straight through the origin.

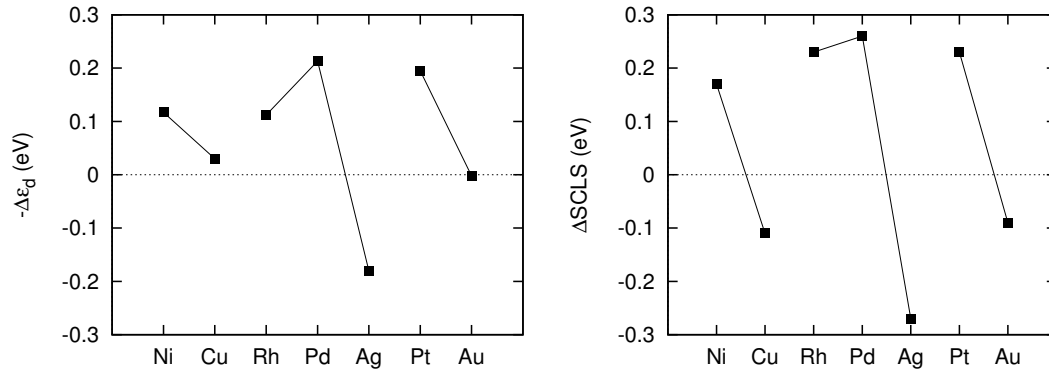


**Figure 4.11:** Shift of d-band centre (left) and chemical shift (right) for O on (100) surfaces.

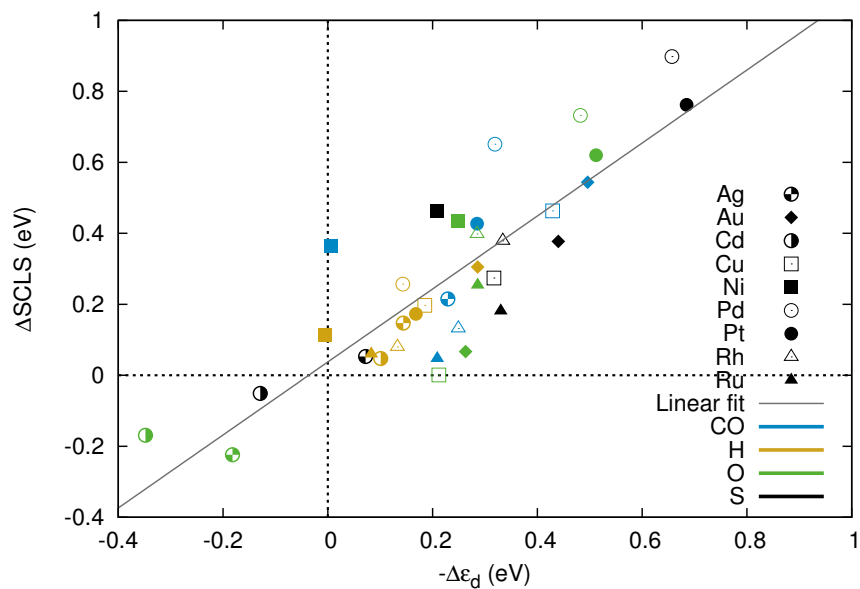


**Figure 4.12:**  $\Delta SCLS$  against  $-\Delta\varepsilon_d$  for (111) surfaces, with all adsorbates and metals included.

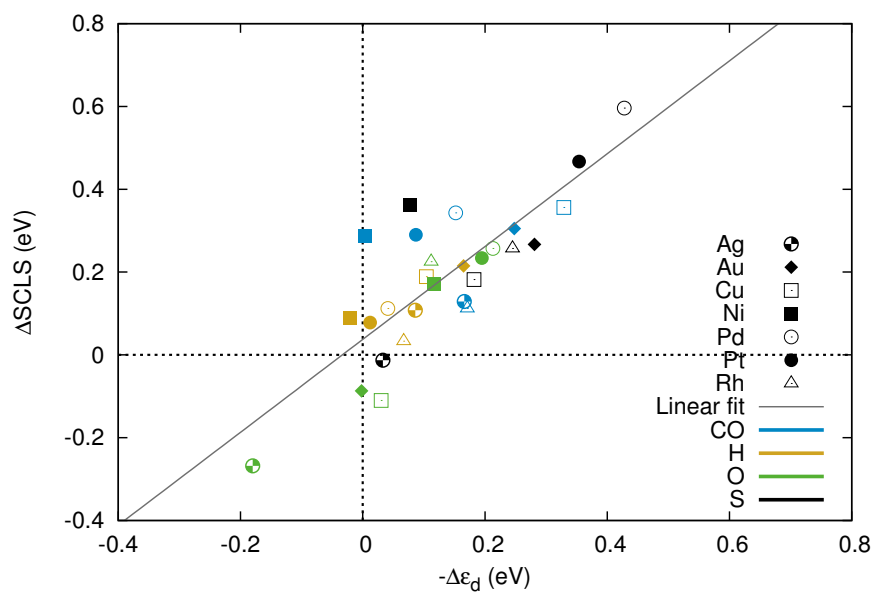


**Figure 4.13:**  $\Delta SCLS$  against  $-\Delta\varepsilon_d$  for (100) surfaces.

# Chapter 5

## Discussion

### 5.1 Results

For the adsorption energy calculations where bridge adsorbates moved into a hollow site, there could possibly still be a metastable bridge site. The adsorbate does not stay put if the initial position is too far from the metastable position, and if it starts moving it continues to relax into the lower energy hollow site. A way to circumvent this is to first relax the setup with a constraint that forces the adsorbate to move only in the direction perpendicular to the surface.

The convergence test showed that we needed 9 layers to achieve converged core level shifts. By choosing the reference atom off-centre but still below the surface, the number of simulated atoms can be greatly reduced. For instance, a 6 layer slab may be thick enough if the bulk reference is chosen from the second to last layer.

The clean surface values are very close to high resolution experimental results in some investigated cases. The Ru value of  $-0.369$  eV closely matches the experimental value of  $-0.366 \pm 10$  eV reported by [26], and the Rh value of  $-0.481$  eV matches  $-0.485 \pm 20$  eV by [27].

To get a match of this kind with adsorbates is difficult since the shifted peak consists of contributions from unequal atoms at the surface. Old experimental data does not have high enough resolution to distinguish between them.

The d-band shift matches the change in SCLS upon adsorption very well. The change in d-band energies is reflected not only by the change in electrostatics, but also by the ability to screen as seen in the DOS [28]. The trends when the SCLS is plotted along the filling of d-band can certainly be explained by the fact that more antibonding states are occupied for the later elements [28]. That the SCLS are larger for the (100) surface is expected, since the change in coordination number is larger than for the (111) surface. The dependence on coordination number change is not constant among elements, since

the bonding nature and hybridisation is different. The change in coordination is therefore more “enjoyable” for some elements than others.

## 5.2 Method

Since we only look at energy differences, many of the systematic errors from the methods (e.g. estimations in functionals) are decreased. However, as in all calculations that rely on pseudopotentials, there is a limitation in applications of transferability of the pseudopotential – the potential is static with respect to changes in the valence.

Convergence of relaxations for some elements (Rh, Cd and In in particular) may require a lower force threshold to reach the equilibrium. Since the VASP manual recommends using force criteria, that is how this work is done. A better option could be to use an energy convergence criterion.

One important conclusion from trying to handle the data in spreadsheets is that they should not be used. LibreOffice had bugs causing display of faulty information. Excel had similar issues and I would strongly recommend against using it, although the Windows version is better than the used Mac version. If I were to start again, I would use a small relational database such as SQLite, which plugs easily into the Python environment already in use.

Using the software VESTA[29] made visualisation of structures much easier than it was with the tools VMD and Povray, to which ASE has links.

## 5.3 Further studies

Since indium has a different surface structure than the other metals, the framework developed for the rest of the study was not straightforwardly applicable (for instance there is as of today no automatic generation of slabs in ASE). Adsorption energies and core level shifts could be investigated continuing from the found surface structures – In(001) resemble the fcc(100) and In(101) the fcc(111) facet (Figure 4.1). These are also the two most energetically stable surfaces.

The SCLS is related to cohesive energy and to surface energy[5]. Comparing the shifts of clean surfaces with these quantities would be interesting. The chemical shift is related to binding, so relating  $\Delta$ SCLS to the adsorption energies is equally important.

Most of this study and many others are focused on what happens when moving along the transition series. Further studies of what happens when moving down the groups could be done to verify the trend found for the Ni and Cu groups.

In addition to comparing the chemical d-band shift of surface atoms with the difference in surface shifts  $\Delta$ SCLS, the d-band shift between bulk and surface can be compared with the values of the SCLS both with and without adsorbates.

The atoms in the (111) surfaces that are *not* directly bound to adsorbates are also affected, both by the adsorbates and by the other surface atoms which are no longer neutral. The shifts of these atoms could be investigated in the same way as the other shifts reported.

The core hole “coverage” is kept at 0.25, the lowest possible with a  $2 \times 2$  unit cell. Since the experimental coverage is probably lower, it may be fruitful to increase the surface cell size. On the other hand, an increased coverage directly affects coordination as well as which sites become preferred. For instance CO sits in top position at low coverage such as 0.25 but also occupies hollow sites at 0.5 [30], thus comparisons with experiments can become more meaningful if calculations are done at higher coverage. It would also show if the trends are stronger or weaker with higher coverage.



## Chapter 6

# Conclusion

Studies of chemical bonding with X-ray photoelectron spectroscopy can determine shifts of core electron binding energies between atoms in different settings. The experimental analysis is often aided by electronic structure calculations to gain additional insight into what the contributions to the spectrum are.

In this thesis, the shift in core electron binding energy of late transition metals has been studied using density functional theory. The change in binding energy for surface atoms upon adsorption of oxygen, sulphur, carbon monoxide and hydrogen was treated.

Known trends in core level shifts have been reproduced. The shifts of clean surfaces are found to match experiments very well. Trends in shift between bulk and surface as well as upon adsorption have also been found. Influence of coordination number on the shift is clearly seen, but the effect depends on the element in question. The surface shifts are less negative for higher atomic numbers. Oxidation of Ni-group metals gives large positive shifts, and sulphur adsorption gives even larger.

Convergence of surface core level shifts to within 0.03 eV requires 3 layers *between* the surface layer and the bulk reference layer. The adsorbates cause polarisation of the first layers that otherwise affects the reference atom.

The method of regarding charge transfer alone as a dominating cause for the core level shift does not give much insight, as was shown by Bader analysis. The d-band shift is known to correlate with a core level shift in general and matches the change in surface shift upon adsorption with an almost 1:1 correspondence.

To conclude, many core level shifts have been calculated and data for comparison with high resolution experiments are made available. Continued analysis will be done on the findings, and hopefully further decomposition into the mechanisms contributing to the shifts can be made.



# Bibliography

- [1] S. Hagström, C. Nordling, K. Siegbahn, Electron spectroscopy for chemical analyses, *Physics Letters* 9 (1964) 235 – 236.
- [2] U. Gelius, E. Basilier, S. Svensson, T. Bergmark, K. Siegbahn, A high resolution ESCA instrument with X-ray monochromator for gases and solids, *Journal of Electron Spectroscopy and Related Phenomena* 2 (1973) 405 – 434.
- [3] H. Grönbeck, S. Klacar, N. M. Martin, A. Hellman, E. Lundgren, J. N. Andersen, Mechanism for reversed photoemission core-level shifts of oxidized Ag, *Phys. Rev. B* 85 (2012) 115445.
- [4] P. S. Bagus, F. Illas, G. Pacchioni, F. Parmigiani, Mechanisms responsible for chemical shifts of core-level binding energies and their relationship to chemical bonding, *Journal of Electron Spectroscopy and Related Phenomena* 100 (1999) 215 – 236.
- [5] B. Johansson, N. Mårtensson, Core-level binding-energy shifts for the metallic elements, *Phys. Rev. B* 21 (1980) 4427–4457.
- [6] N. Mårtensson, A. Nilsson, On the origin of core-level binding energy shifts, *Journal of Electron Spectroscopy and Related Phenomena* 75 (1995) 209 – 223.
- [7] J. F. Moulder, W. F. Stickle, P. E. Sobol, K. D. Bomben, *Handbook of X-ray photoelectron spectroscopy*, Perkin-Elmer corp., Physical electronics division, Eden Prairie, MN, 1992.
- [8] P. Hohenberg, W. Kohn, Inhomogeneous electron gas, *Phys. Rev.* 136 (1964) B864–B871.
- [9] W. Kohn, L. J. Sham, Self-consistent equations including exchange and correlation effects, *Phys. Rev.* 140 (1965) A1133–A1138.
- [10] L. Hedin, B. I. Lundqvist, S. Lundqvist, Local exchange-correlation potentials, *Solid State Communications* 9 (1971) 537 – 541.
- [11] J. P. Perdew, K. Burke, M. Ernzerhof, Generalized gradient approximation made simple, *Phys. Rev. Lett.* 77 (1996) 3865–3868.
- [12] P. E. Blöchl, Projector augmented-wave method, *Phys. Rev. B* 50 (1994) 17953–17979.
- [13] J. Thijssen, *Computational Physics*, 2nd Edition, Cambridge University Press, Cambridge, UK, 2007.

- [14] K. Burke, L. O. Wagner, DFT in a nutshell, *International Journal of Quantum Chemistry* 113 (2013) 96–101.
- [15] VASP manual (05 2013).  
URL <http://cms.mpi.univie.ac.at/VASP/>
- [16] P. Pulay, Convergence acceleration of iterative sequences. The case of SCF iteration, *Chemical Physics Letters* 73 (1980) 393 – 398.
- [17] A. B. Alchagirov, J. P. Perdew, J. C. Boettger, R. C. Albers, C. Fiolhais, Reply to “Comment on ‘Energy and pressure versus volume: Equations of state motivated by the stabilized jellium model’ ”, *Phys. Rev. B* 67 (2003) 026103.
- [18] R. Bader, *Atoms in Molecules: A Quantum Theory*, Oxford University Press, New York, 1990.
- [19] W. Tang, E. Sanville, G. Henkelman, A grid-based Bader analysis algorithm without lattice bias, *Journal of Physics: Condensed Matter* 21 (2009) 084204.
- [20] F. Tran, R. Laskowski, P. Blaha, K. Schwarz, Performance on molecules, surfaces, and solids of the Wu-Cohen GGA exchange-correlation energy functional, *Phys. Rev. B* 75 (2007) 115131.
- [21] C. Kittel, *Introduction to Solid State Physics*, 8th Edition, John Wiley & Sons, 2005.
- [22] A. Zoroddu, F. Bernardini, P. Ruggerone, V. Fiorentini, First-principles prediction of structure, energetics, formation enthalpy, elastic constants, polarization, and piezoelectric constants of AlN, GaN, and InN: Comparison of local and gradient-corrected density-functional theory, *Phys. Rev. B* 64 (2001) 045208.
- [23] P. Janthon, S. M. Kozlov, F. Viñes, J. Limtrakul, F. Illas, Establishing the accuracy of broadly used density functionals in describing bulk properties of transition metals, *Journal of Chemical Theory and Computation* 9 (2013) 1631–1640.
- [24] J. Paier, M. Marsman, K. Hummer, G. Kresse, I. C. Gerber, J. G. Ángyán, Erratum: “Screened hybrid density functionals applied to solids” [*JCP* 124, 154709 (2006)], *The Journal of Chemical Physics* 125 (2006) 249901.
- [25] W. Tyson, W. Miller, Surface free energies of solid metals: Estimation from liquid surface tension measurements, *Surface Science* 62 (1977) 267 – 276.
- [26] S. Lizzit, A. Baraldi, A. Groso, K. Reuter, M. V. Ganduglia-Pirovano, C. Stampfl, M. Scheffler, M. Stichler, C. Keller, W. Wurth, D. Menzel, Surface core-level shifts of clean and oxygen-covered Ru(0001), *Phys. Rev. B* 63 (2001) 205419.
- [27] M. V. Ganduglia-Pirovano, M. Scheffler, A. Baraldi, S. Lizzit, G. Comelli, G. Paolucci, R. Rosei, Oxygen-induced Rh  $3d_{5/2}$  surface core-level shifts on Rh(111), *Phys. Rev. B* 63 (2001) 205415.

- [28] M. Aldén, I. A. Abrikosov, B. Johansson, N. M. Rosengaard, H. L. Skriver, Self-consistent green's-function technique for bulk and surface impurity calculations: Surface core-level shifts by complete screening, *Phys. Rev. B* 50 (1994) 5131–5146.
- [29] K. Momma, F. Izumi, *VESTA3* for three-dimensional visualization of crystal, volumetric and morphology data, *Journal of Applied Crystallography* 44 (2011) 1272–1276.
- [30] M. Birgersson, C.-O. Almbladh, M. Borg, J. N. Andersen, Density-functional theory applied to Rh(111) and CO/Rh(111) systems: Geometries, energies, and chemical shifts, *Phys. Rev. B* 67 (2003) 045402.



# Appendix A

## Adsorption energies

**Tables A.1–A.8:** Adsorption energies  $F$  in eV are calculated according to equation 3.1. They are given with both free atoms and molecules as reference, where the latter includes the dissociation energy. The tables are sorted with strongest bindings first for each metal. For CO, the C–O bond length  $d$  in Å is given in the last column. Gas phase CO is also calculated and has  $d = 1.143$ .

**Table A.1:** CO on (100)

	Site	$F_{\text{molec}}$	$d$
Ag	top	-0.254	1.15
	bridge	-0.222	1.16
	hollow	-0.053	1.18
Au	bridge	-0.543	1.17
	top	-0.441	1.15
	hollow	-0.097	1.18
Cu	bridge	-0.846	1.17
	top	-0.832	1.16
	hollow	-0.817	1.20
Ni	hollow	-1.917	1.21
	bridge	-1.845	1.18
	top	-1.666	1.16
Pd	bridge	-1.872	1.18
	hollow	-1.837	1.20
	top	-1.452	1.16
Pt	bridge	-2.123	1.18
	top	-1.929	1.16
	hollow	-1.652	1.20
Rh	bridge	-1.990	1.18
	top	-1.901	1.17
	hollow	-1.875	1.21

**Table A.2:** H on (100)

	Site	$F_{\text{molec}}$	$F_{\text{atom}}$
Ag	hollow	0.318	-1.947
	bridge	0.334	-1.931
	top	0.788	-1.477
Au	bridge	0.047	-2.218
	hollow	0.369	-1.896
	top	0.392	-1.874
Cu	hollow	-0.118	-2.384
	bridge	-0.038	-2.303
	top	0.436	-1.829
Ni	hollow	-0.526	-2.792
	bridge	-0.407	-2.673
	top	0.046	-2.219
Pd	hollow	-0.462	-2.727
	bridge	-0.433	-2.698
	top	0.022	-2.243
Pt	bridge	-0.669	-2.934
	top	-0.465	-2.730
	hollow	-0.336	-2.602
Rh	bridge	-0.510	-2.776
	hollow	-0.493	-2.759
	top	-0.206	-2.472

**Table A.3:** O on (100)

	Site	$F_{\text{molec}}$	$F_{\text{atom}}$
Ag	hollow	-0.780	-3.810
	bridge	0.029	-3.000
Au	hollow	0.081	-2.948
	bridge	0.127	-2.902
Cu	hollow	-2.010	-5.040
	bridge	-1.107	-4.136
Ni	hollow	-2.623	-5.652
	bridge	-1.912	-4.942
Pd	hollow	-1.273	-4.303
	bridge	-0.886	-3.916
Pt	bridge	-1.189	-4.218
	hollow	-0.907	-3.937
Rh	hollow	-2.018	-5.048
	bridge	-1.830	-4.860

**Table A.4:** S on (100)

	Site	$F_{\text{molec}}$	$F_{\text{atom}}$
Ag	hollow	-1.494	-3.992
	bridge	-0.661	-3.159
Au	hollow	-1.220	-3.718
	bridge	-0.679	-3.177
Cu	hollow	-2.414	-4.912
	bridge	-1.433	-3.931
Ni	hollow	-3.315	-5.813
	bridge	-2.197	-4.696
Pd	hollow	-3.025	-5.523
	bridge	-1.725	-4.223
Pt	hollow	-3.163	-5.661
	bridge	-2.121	-4.619
Rh	hollow	-3.458	-5.956
	bridge	-2.367	-4.866

**Table A.5:** CO on (111)

	Site	$F_{\text{molec}}$	$d$
Ag	top	-0.187	1.15
	fcc	-0.168	1.17
	hcp	-0.161	1.17
	bridge	-0.143	1.17
Au	bridge	-0.302	1.17
	fcc	-0.297	1.18
	top	-0.264	1.15
Cd	hcp	-0.254	1.18
	all	does not bind	
Cu	fcc	-0.831	1.18
	hcp	-0.811	1.18
	bridge	-0.750	1.18
Ni	top	-0.674	1.16
	hcp	-1.897	1.19
	fcc	-1.875	1.19
	bridge	-1.781	1.18
Pd	top	-1.542	1.16
	hcp	-1.974	1.19
	fcc	-1.951	1.19
Pt	bridge	-1.797	1.18
	top	-1.380	1.16
	hcp	-1.797	1.19
Rh	fcc	-1.792	1.19
	bridge	-1.782	1.18
	top	-1.666	1.16
Ru	hcp	-1.975	1.19
	top	-1.909	1.16
Ru	fcc	-1.876	1.19
	bridge	-1.872	1.18
	hcp	-1.871	1.20
Ru	top	-1.870	1.17
	bridge	falls to hollow	
	fcc	-1.688	1.19

**Table A.6:** H on (111)

	Site	$F_{\text{molec}}$	$F_{\text{atom}}$
Ag	fcc	0.153	-2.112
	hcp	0.169	-2.097
	bridge	0.281	-1.984
	top	0.681	-1.585
Au	fcc	0.090	-2.176
	hcp	0.134	-2.131
	top	0.330	-1.935
	bridge	falls to hollow	
Cd	bridge	0.779	-1.486
	top	0.811	-1.454
	fcc	0.836	-1.429
	hcp	0.905	-1.361
Cu	fcc	-0.207	-2.472
	hcp	-0.191	-2.456
	bridge	-0.066	-2.332
	top	0.398	-1.867
Ni	fcc	-0.564	-2.829
	hcp	-0.552	-2.818
	bridge	-0.420	-2.685
	top	0.030	-2.236
Pd	fcc	-0.564	-2.829
	hcp	-0.528	-2.793
	bridge	-0.423	-2.688
	top	-0.045	-2.310
Pt	top	-0.494	-2.759
	fcc	-0.484	-2.749
	bridge	-0.444	-2.710
	hcp	-0.442	-2.707
Rh	fcc	-0.545	-2.810
	hcp	-0.530	-2.796
	bridge	-0.436	-2.701
	top	-0.205	-2.471
Ru	fcc	-0.645	-2.910
	hcp	-0.578	-2.843
	bridge	-0.485	-2.750
	top	-0.172	-2.437

**Table A.7:** O on (111)

	Site	$F_{\text{molec}}$	$F_{\text{atom}}$
Ag	fcc	-0.511	-3.541
	hcp	-0.404	-3.434
	bridge	-0.177	-3.206
Au	fcc	-0.084	-3.114
	hcp	0.178	-2.851
	bridge	0.401	-2.629
Cd	hcp	-1.253	-4.283
	fcc	-1.146	-4.176
Cu	bridge	falls to hollow	
	fcc	-1.668	-4.698
	hcp	-1.544	-4.573
Ni	bridge	-1.249	-4.278
	fcc	-2.346	-5.376
	hcp	-2.267	-5.297
Pd	bridge	-1.782	-4.812
	fcc	-1.305	-4.335
	hcp	-1.142	-4.172
Pt	bridge	-0.767	-3.797
	fcc	-1.225	-4.255
	hcp	-0.782	-3.811
Rh	bridge	-0.611	-3.641
	fcc	-2.056	-5.086
	hcp	-1.985	-5.015
Ru	bridge	-1.535	-4.564
	hcp	-3.026	-6.056
	fcc	-2.386	-5.416
	bridge	-2.207	-5.237

A. ADSORPTION ENERGIES

---

**Table A.8:** S on (111)

	Site	$F_{\text{molec}}$	$F_{\text{atom}}$
	fcc	-1.099	-3.597
Ag	hcp	-1.035	-3.533
	bridge	-0.917	-3.415
	fcc	-1.032	-3.530
Au	hcp	-0.824	-3.323
	bridge	-0.575	-3.073
	hcp	-0.989	-3.487
Cd	fcc	-0.915	-3.413
	bridge	falls to hollow	
	fcc	-1.859	-4.358
Cu	hcp	-1.807	-4.306
	bridge	-1.686	-4.184
	fcc	-2.600	-5.098
Ni	hcp	-2.559	-5.057
	bridge	-2.322	-4.820
	fcc	-2.339	-4.837
Pd	hcp	-2.312	-4.810
	bridge	-1.960	-4.458
	fcc	-2.594	-5.092
Pt	hcp	-2.380	-4.878
	bridge	-1.928	-4.426
	fcc	-2.887	-5.385
Rh	hcp	-2.880	-5.378
	bridge	-2.416	-4.914
	hcp	-3.284	-5.782
Ru	fcc	-3.031	-5.529
	bridge	-2.755	-5.254